NAVAL
POSTGRADUATE
SCHOOL

MONTEREY, CALIFORNIA

THESIS

COLD FLOW DRAG MEASUREMENT AND NUMERICAL PERFORMANCE PREDICTION OF A MINIATURE RAMJET AT MACH 4

by

Wee Teik Khoo

December 2003

Thesis Advisor:	Garth V. Hobson
Second Reader:	Raymond P. Shreeve

Approved for public release; distribution is unlimited

THIS PAGE INTENTIONALLY LEFT BLANK

REPORT DOCUMENTATION PAGE			Form Approved OMB No. 0704-0188
Public reporting burden for this collection of information is estimated to average 1 hour per response, including the time for reviewing instruction, searching existing data sources, gathering and maintaining the data needed, and completing and reviewing the collection of information. Send comments regarding this burden estimate or any other aspect of this collection of information, including suggestions for reducing this burden, to Washington headquarters Services, Directorate for Information Operations and Reports, 1215 Jefferson Davis Highway, Suite 1204, Arlington, VA 22202-4302, and to the Office of Management and Budget, Paperwork Reduction Project (0704-0188) Washington DC 20503.			
1. AGENCY USE ONLY *(Leave blank)*	**2. REPORT DATE** December 2003	**3. REPORT TYPE AND DATES COVERED** Master's Thesis	
4. TITLE AND SUBTITLE: Title (Mix case letters) Cold Flow Drag Measurement and Numerical Performance Prediction of a Miniature Ramjet at Mach 4			**5. FUNDING NUMBERS**
6. AUTHOR(S) Wee Teik Khoo			
7. PERFORMING ORGANIZATION NAME(S) AND ADDRESS(ES) Naval Postgraduate School Monterey, CA 93943-5000			**8. PERFORMING ORGANIZATION REPORT NUMBER**
9. SPONSORING /MONITORING AGENCY NAME(S) AND ADDRESS(ES) N/A			**10. SPONSORING/MONITORING AGENCY REPORT NUMBER**
11. SUPPLEMENTARY NOTES The views expressed in this thesis are those of the author and do not reflect the official policy or position of the Department of Defense or the U.S. Government.			
12a. DISTRIBUTION / AVAILABILITY STATEMENT Approved for public release; distribution is unlimited			**12b. DISTRIBUTION CODE**

13. ABSTRACT (maximum 200 words)

Experimentation was carried out in a supersonic wind tunnel to investigate the drag force on a miniature ramjet when subjected to Mach 4 flow. CFDRC-FASTRAN, a numerical flow solver developed for the analysis of high-speed flows was used to model the performance of the miniature ramjet. To reduce computational time, a 2D axisymmetric model of the ramjet was developed to investigate the shock angles over the intake and the results were compared with the experiment. A 3D axisymmetric flow model was developed to investigate the fuel mixing which was injected into the ramjet from the nose cone and from the struts, which held the centerbody in place. Finally a 2D model was developed to investigate the combustion of the propane fuel, which was injected from the struts. For all of the simulations a two-equation, $k-\omega$, turbulence model was used. Further investigation is needed at supersonic freestream conditions in the simulation of the combustion process.

14. SUBJECT TERMS Mach 4, Ramjet, Drag measurement, Turbulence modeling, Simulation			**15. NUMBER OF PAGES** 85
			16. PRICE CODE
17. SECURITY CLASSIFICATION OF REPORT Unclassified	**18. SECURITY CLASSIFICATION OF THIS PAGE** Unclassified	**19. SECURITY CLASSIFICATION OF ABSTRACT** Unclassified	**20. LIMITATION OF ABSTRACT** UL

NSN 7540-01-280-5500 Standard Form 298 (Rev. 2-89)
Prescribed by ANSI Std. 239-18

THIS PAGE INTENTIONALLY LEFT BLANK

Approved for public release; distribution is unlimited

COLD FLOW DRAG MEASUREMNT AND NUMERICAL PERFORMANCE PREDICTION OF A MINIATURE RAMJET AT MACH 4

Wee Teik Khoo
Civilian, Singapore Ministry of Defense
B.Eng., University of Leeds, 1996

Submitted in partial fulfillment of the
requirements for the degree of

**MASTER OF SCIENCE IN ENGINEERING SCIENCE
(MECHANICAL ENGINEERING)**

from the

**NAVAL POSTGRADUATE SCHOOL
Dec 2003**

Author: Wee Teik Khoo

Approved by: Professor Garth V. Hobson
Thesis Advisor

Professor Raymond P. Shreeve
Second Reader

Professor Anthony J. Healey
Chairman, Department of Mechanical and Astronautical Engineering

THIS PAGE INTENTIONALLY LEFT BLANK

ABSTRACT

Experimentation was carried out in a supersonic wind tunnel to investigate the drag force on a miniature ramjet when subjected to Mach 4 flow. CFDRC-FASTRAN, a numerical flow solver developed for the analysis of high-speed flows was used to model the performance of the miniature ramjet. To reduce computational time, a 2D axisymmetric model of the ramjet was developed to investigate the shock angles over the intake and the results were compared with the experiment. A 3D axisymmetric flow model was developed to investigate the fuel mixing which was injected into the ramjet from the nose cone and from the struts, which held the centerbody in place. Finally a 2D model was developed to investigate the combustion of the propane fuel, which was injected from the struts. For all of the simulations a two-equation, $k-\omega$, turbulence model was used. Further investigation is needed at supersonic freestream conditions in the simulation of the combustion process.

THIS PAGE INTENTIONALLY LEFT BLANK

TABLE OF CONTENTS

LIST OF FIGURES

LIST OF TABLES

THIS PAGE INTENTIONALLY LEFT BLANK

ACKNOWLEDGMENTS

I would like to extend my sincere appreciation in acknowledging several people whose efforts greatly contributed to the successful completion of this thesis.

Thanks to Mr. Rick Still, Mr John Gibson and Mr. Doug Seivwright at the Turbopropulsion Lab for their help and assistance with the wind tunnel testing. Most grateful thanks to Mr. Doug Seivwright, for his great skill in bonding the strain gages onto the flexure.

Most notable thanks to my advisor Dr. Garth Hobson of the Department of Mechanical and Astronautical Engineering for providing the opportunity to work with him.

Finally I would like to express my gratitude to my wife, Joanne Lim and my son, Alastair Khoo for their understanding and support while undertaking this research.

THIS PAGE INTENTIONALLY LEFT BLANK

I. INTRODUCTION

Ramjet powered missiles have been used successfully since the 1950's [1] with the most impressive being the Bomarc missile. It was first deployed in 1955 as a ground-to-air defense system. Its take-off weight was 16000 lbf (71 kN) and it was 43.6 ft (13.3 m) long. The ramjet engine could propel it about 435 miles (700 km) at an altitude of 69 kft (21 km) and a Mach number of 3.0. As of 1990, six military ramjet missiles were operational. Two of these were so called first-generation missiles; namely, Britain's Bloodhound and China's variant of the Bloodhound, the HY-3/C101, both used for surface-to-air combat. Another two were second generation missiles; namely, Britain's Sea Dart and the former Soviet Union SA-4 Ganef, both featuring internal liquid fuel ramjets and tandem solid propellant booster rockets. Both were also used for surface-to-air combat. The latter had a range in excess of about 43 miles (70 km) at an altitude of about 79 kft (24 km) and a Mach number of about 3.5. The remaining two were third generation missiles; namely, the former Soviet Union's SA-6 Gainful and France's ASMP ($Air-sol-Moyenne-Porte\acute{e}$). The ASMP featured an integral solid rocket booster contained within the space that becomes the ramjet combustion chamber after the boost phase. It was also the first air-to-surface ramjet missile to be deployed, and it was the highest performance missile in the world for its size and weight. It had a range of 156 miles (250 km) and a Mach number of about 3 [1].

With the increasing interest in micro technology it is now possible to design and analize miniature ramjets. A miniaturized ramjet is a relatively new idea that might have limited military application. At present, work in the area of ramjets involves the development of a scramjet to power a 4 inche diameter (101mm) kinetic energy tank round. This contrasts with the unpowered kinetic energy tank round which slows down and looses penetrating power due to aerodynamic drag. In principle, a scramjet powered round could sustain its tank-penetration power over long ranges, or enable a smaller, lighter gun to achieve the same result [2]. The development of a miniature ramjet has the potential to

be integrated into a miniature missile system that could be mounted on a Unmanned Combat Air Vehicle (UCAV) or Unmanned Land Vehicle (ULV). It could also be used as a hand-held, high-speed projectile against armored vehicles at a further standoff distance of engagement. A miniature ramjet can also provide the supersonic propulsion system for a new class of Micro Air Vehicles (MAV). But before these concepts can be fulfilled, study into miniature ramjet performance is vital.

The current project is a follow on to work undertaken by Ferguson [3] who designed a miniature ramjet to operate at Mach 4. The objective of the project is to evaluate the performance of the miniature ramjet at it's designed Mach number since there is limited data available in the open literature. The design consisted of 5 major components namely; an intake, a combustion chamber, a nozzle, four struts and a pair of flexures. The inlet cone was designed as a 2-shock external compression system with an oblique shock at the tip of the inlet cone and a normal shock at the lip of the intake. The inlet was followed by a constant area combustion chamber, and the final nozzle had an area expansion ratio of 2.789. Internal struts had two functions; they acted as structural members for the nose cone, and served to provide fuel to the combustion chamber and to four forward fuel injection ports near the tip of the nose cone. A pair of flexures were designed for drag and thrust measurement when the ramjet was tested in a supersonic wind tunnel with a cross section of 4 inches by 4 inches.

The present thesis describes the experimental measurement of the drag force produced by the Mach 4 flow on the miniature ramjet and compares those data with numerical and theoretical predictions. The major portion of the work was devoted to investigating and predicting the performance of the ramjet using computational fluid dynamics (CFD). With the advance in computational power, numerical investigations have in recent years become less expensive; but in some cases the existing models do not allow the simulation of the complex physical processes with appropriate accuracy. The present study used CFDRC-FASTRAN, which is a flow solver developed to simulate and analyze compressible flow problems, including combustion of various gases. It had the

capability to handle the mixing of chemical species as well as chemical reaction. The modeling of supersonic flow with shock waves and complicated shock-boundary layer interactions would require very fine meshes, which would increase the necessary computation time remarkably. Using models with chemistry included would make the simulation almost impossible for the real 3-dimension geometry because of the excessive memory and computational time required. Furthermore, since the ramjet was designed for high-speed flow, the physics describing the flow would be complex, and mostly fall within the turbulent regime. A two-equation (k-ω) turbulence model was used to carry out the simulation. In order to cut down the computational time required, an axisymmetric model was developed to investigate the shock angle profile and compare it with experimental results. A three-dimensional model, with coarser grids, was developed for prediction of the fuel-air mixture with the current design of the fuel injector ports. Finally a 2D model was developed to investigate the combustion of the propane gas, which was injected from the struts into the combustion chamber of the ramjet. Simulation allows a detailed model of the velocity and temperature field and species concentrations, which could aid in the design and optimization of the miniature ramjet before expensive experiments are carried out.

THIS PAGE INTENTIONALLY LEFT BLANK

II. DRAG MEASUREMENT

A. METHODOLOY OF DRAG MEASUREMNT

A pair of load flexures were designed by Ferguson [3] to facilitate for the drag (and thrust) measurements within the wind tunnel. The flexures were designed within a modified double wedge airfoil cross section. The model was attached to the vertical walls of the wind tunnel between the horizontally mounted flexures. Figure 1 shows a schematic of the ramjet secured in the wind tunnel by the two flexures.

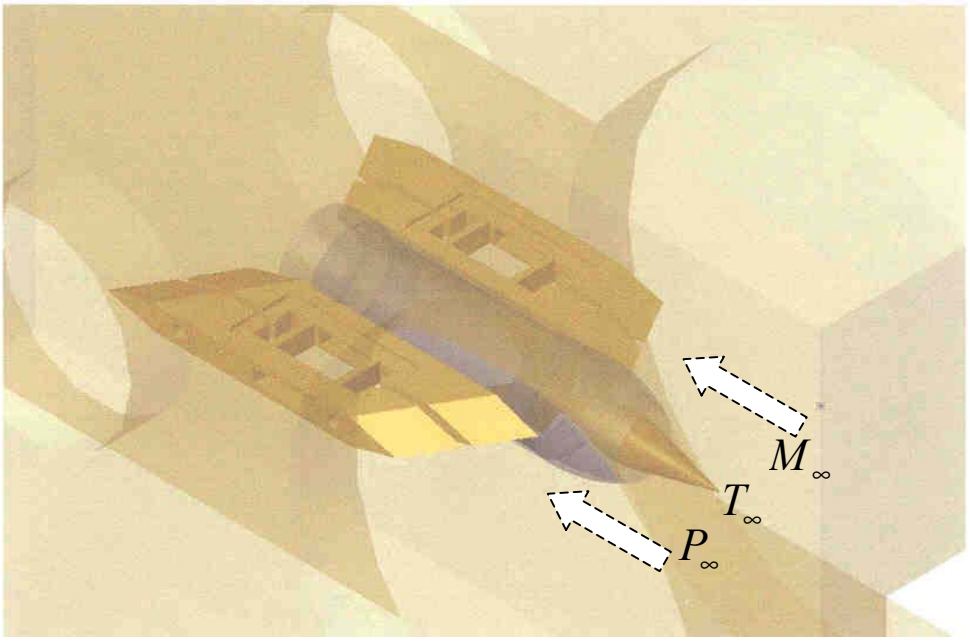

Figure 1. View of ramjet in wind tunnel with flexures

The axial movement of the flexure was achieved by two thin beams of 0.08” (2mm) thickness located within the airfoil sections, which joined both ends of the flexure. In order to measure the drag or thrust, strain gages were bonded to the flexure beams to measure the strain value of each beam under axial loading. In total, four strain gages were required for the pair of flexures.

B. STRUCTURAL ANALYSIS

The low cost and fast computing power possessed by current personal computers (PCs) allow the quick reconfiguration of geometries for analysis during the design phase. A Finite Element Method (FEM) code MSC-PATRAN/NASTRAN, was used to determine the structural integrity of the flexure as well as to identify the maximum strain level that the flexure beam would experience. The expected maximum axial load was 52lbf (230N) for each flexure, so that an appropriate strain gage could be selected.

MSC. PATRAN/NASTRAN is a computer-aided engineering (CAE) software package. PATRAN was used to model the flexure geometry, create the FEM model and set boundary conditions and loads. The FEM model was then analyzed with NASTRAN and the results finally viewed in PATRAN. Figure 2 show a generic flow sequence in generating a FEM model for analysis.

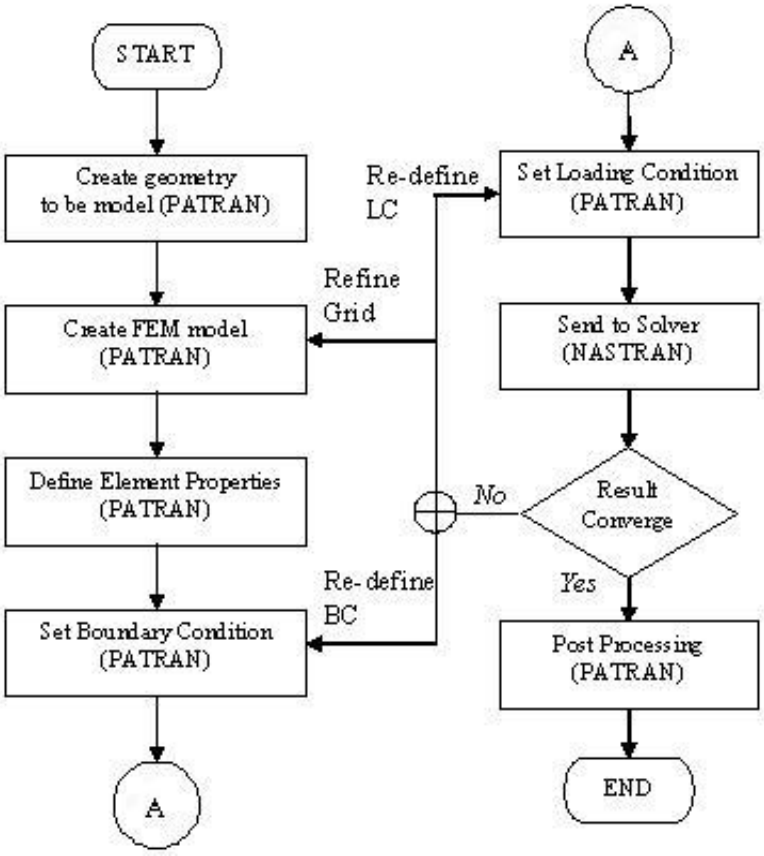

Figure 2. FEM analysis flow chart.

1. FEM Model Set Up

The geometry or the computational domain of the model to be analyzed had to be created. In order to reduce the computational times required, a simplified version of the flexure (Figure 3) was created for the FEM model, using a rectangular shaped model as shown in Figure 4.

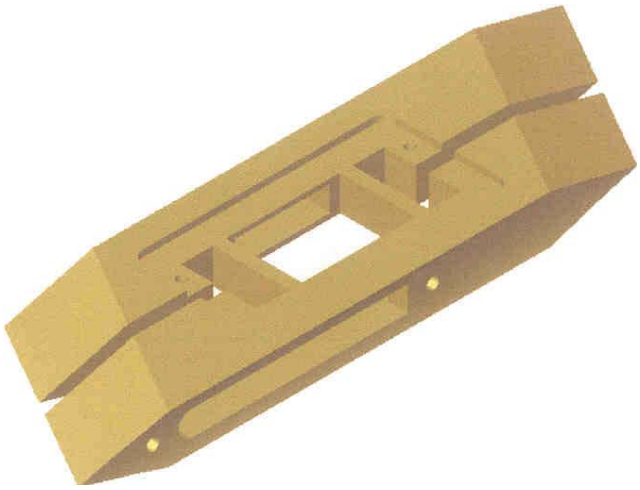

Figure 3. Double modified wedge flexure design.

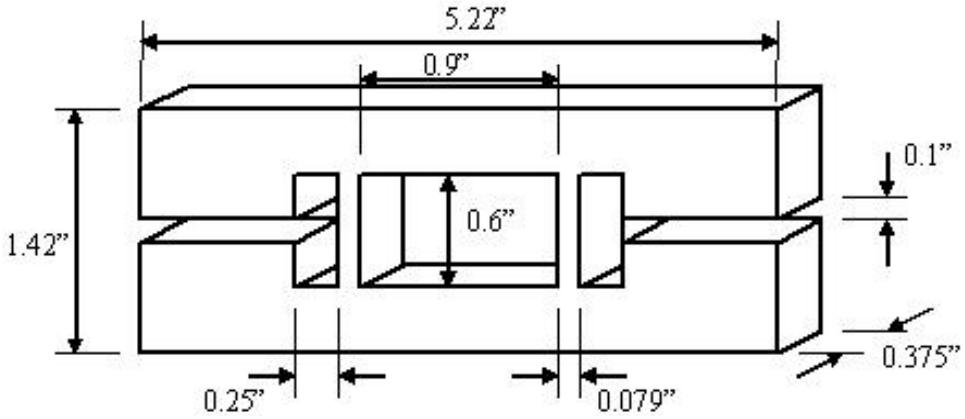

Figure 4. Simplified FEM model of the flexure.

2. FEM Grid Generation

The next step was to generate the grid for the model. Figure 5 shows the grid spacing used in the FEM model. Higher density grids were used at locations where the gradient of the stress distribution was expected to be the greatest. In this case, the stress and axial displacements of the flexure beam were critical.

Coarser grids were used in locations deemed to be less critical which would assist in the reduction of the computational times required. Quad 8 elements were used to create the structured grid, with a total number of cells of 184,000.

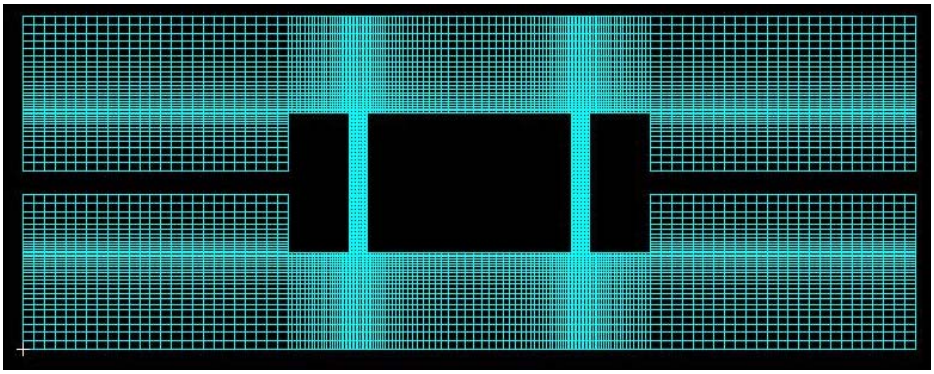

Figure 5. Overall view of grid spacing used for the FEM model.

3. FEM Boundary Conditions

Since one side of the flexure was secured to the wall of the wind tunnel, the boundary condition on that surface was fully constrained, which meant that there was no translation in all directions at that surface. On the opposite surface, the flexure was secured to the ramjet. Drag and thrust acting on the ramjet would be transmitted into force acting on the flexure. The force would be acting either in the forward or backward direction depending on whether it was a drag or thrust. A total force of 52lbf (230N) was the maximum expected load that the flexure would see. This was based on a predicted thrust of 32 lbf (142 N) [3] with a factor of safety of 1.6 applied. Figure 6 show the boundary conditions that were used in the model.

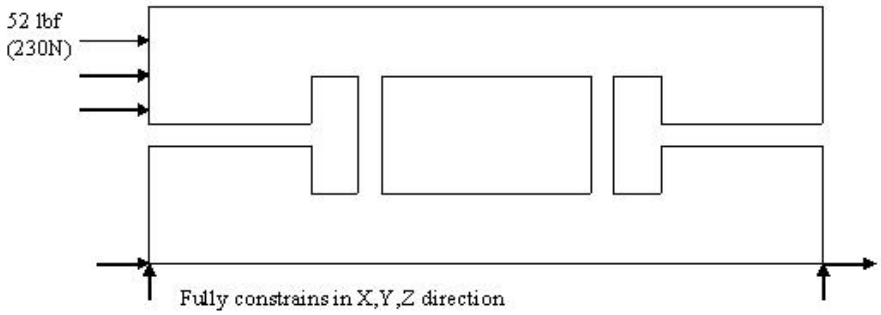

Figure 6. Boundary condition.

4. FEM Post-Processing

The stress distribution along the flexure beam was as expected, with the highest at both corners of the flexure beams. The original design, with a 0.1" (2.54 mm) thick flexure beam, was deemed to be too rigid. A 0.079" (2.0 mm) thick flexure beam was identified as a suitable dimension, after a few simulations were run with various dimensions. The average stress at the mid span of the flexure beam was determined to be approximately 15.2 kpsi (105 MPa). The flexure was machined from a 7000 series aluminum, which had an elastic modulus of 10,153 kpsi (70 GPa) and a Poisson ratio of 0.34. The average strain at the mid span of the flexure beam was calculated to be approximately 1500 micro strain. The maximum deflection was approximately 0.0058" (0.147 mm). Figure 7 is the FEM simulation result, which shows the stress distribution as well as the deflection of the flexure beam. To exaggerate the actual deflection, the displacement was amplified by a factor of 10 times the actual deflection.

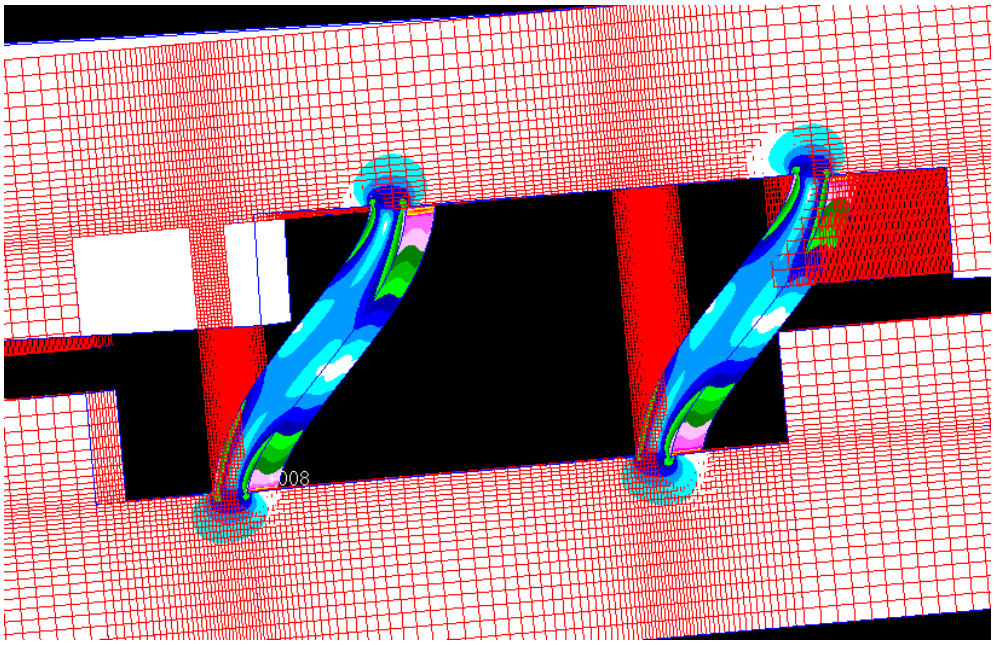

Figure 7. FEM simulation view of the flexure beam under 52 lbf (230N) axial load.

C. STRAIN GAGE INSTALLATION

Ideally the bonding of the strain gage should position the gage at the zone with high stress concentration. Due to the limited space available on the flexure

beam, the strain gages had to be bonded at the mid span of the flexure beam. Figure 8, shows a typical bonding arrangement of a strain gage onto a specimen. Figure 9, shows a photograph which identifies the location where the strain gages were bonded on to the flexure beam.

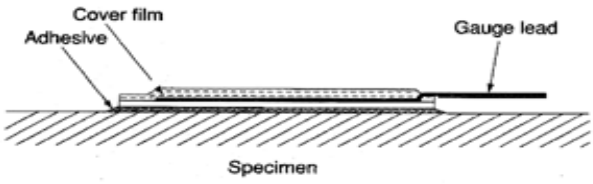

Figure 8. Bonding arrangement for strain gage.

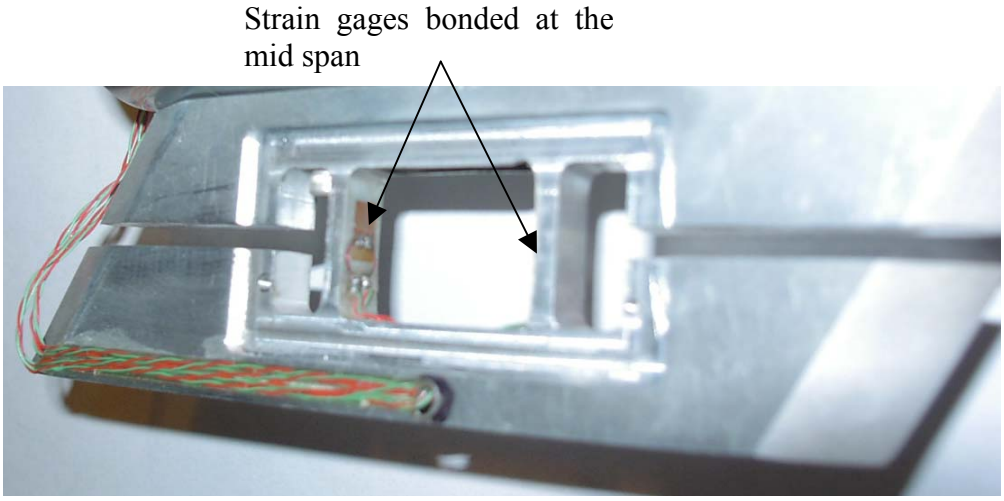

Figure 9. Location of the strain gages on the flexure beam.

D. SUPERSONIC WIND TUNNEL TESTS (SSWT)

These experiments were conducted at the Naval Postgraduate School's (NPS) Gas Dynamic Laboratory (GDL). The SSWT consisted of a Mach 4 two-dimensional convergent-divergent nozzle. The challenge in conducting these experiments lay primary in the available working space inside the 4" by 4" test section (Figure 10). Adding onto the challenge, calibration of the strain gages had to be carried out inside the wind tunnel after securing the miniature ramjet in the test section.

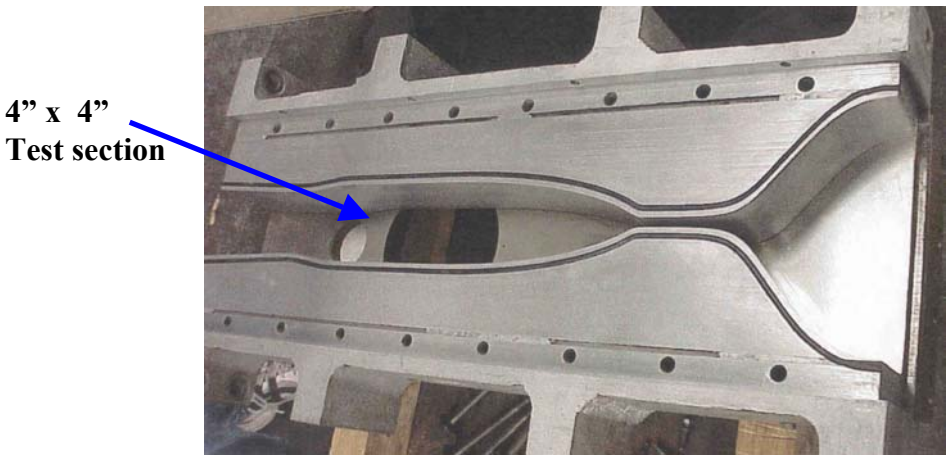

Figure 10. Photograph of the supersonic wind tunnel nozzle and test section.

Air supply from high-pressure (280 psia) storage tanks was valved to the SSWT plenum chamber. The pressure in the plenum ahead of the nozzle was controlled to be 150 psia (1.12 MPa) with the air temperature at that location 58.7 $^{\circ}F$ (288 K). The calculated pressure after the nozzle divergent section was determined to be 1.07 psia (7378 Pa) with the downstream air temperature reduced to –337.3 $^{\circ}F$ (68 K). The sonic velocity was calculated to be 542 ft/s (165.3 m/s) and so the Mach 4 flow produced a velocity of 2169 ft/s (661 m/s). The calculated pressure corresponded to a pressure altitude of 59 kft (18,000 m); however the temperature was less than standard temperature at that altitude by 46 $^{\circ}F$ (149K).

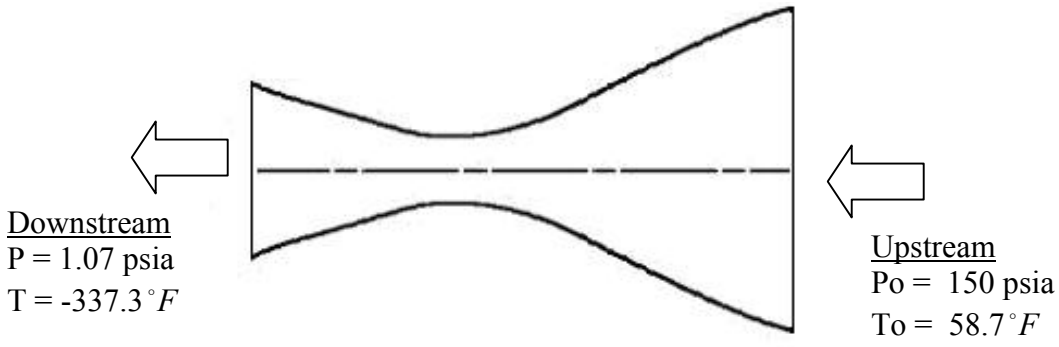

Figure 11. Schematic of a convergent divergent nozzle.

1. Experimental Test Setup

A schematic layout of the supersonic wind tunnel test setup and data acquisition system is shown in Figure 12. The HP9000 series 300 workstation was used to capture the output data from the Data Acquisition System (DAS). A scanning unit (DACU) was used in conjunction with a HP digital voltmeter (DVM) as shown in Figure 13, which received signals through a signal conditioner. The raw data were processed using a computer code written in HP Basic (see appendix D) into a readable engineering format in pound force. The processed data were sent either to the monitor for real time viewing, or the printer, or stored for further data analysis. HP-Interface Bus, IEEE-488, was used to link the DAS, DVM and multi-programmer to the workstation.

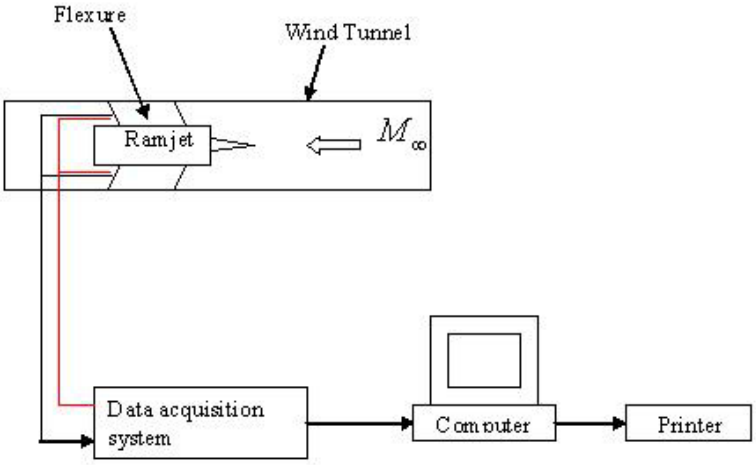

Figure 12. Schematic layout of the test setup.

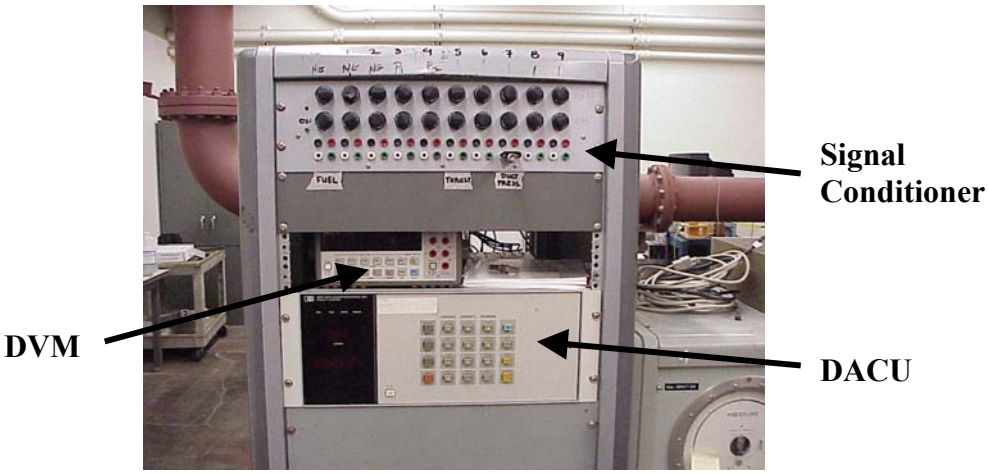

Figure 13. Photograph of the data acquisition system.

2. Calibration of the Flexure Arms

The ramjet mounted with both flexures was secured into the wind tunnel. To ensure that the ramjet body was level, a leveling gage was used. Next, the thrust fixture was mounted such that its internal step was against the lip of the ramjet inlet. The load cell was placed in position with its nipple positioned directly in the groove within the end of the thrust fixture. When everything was in place, the jackscrew was tightened to push against the load cell, as well as the wooden reaction block which was wedged within the wind tunnel nozzle blocks ahead of the test section. Figure 14 shows a photo of the calibration setup inside the wind tunnel.

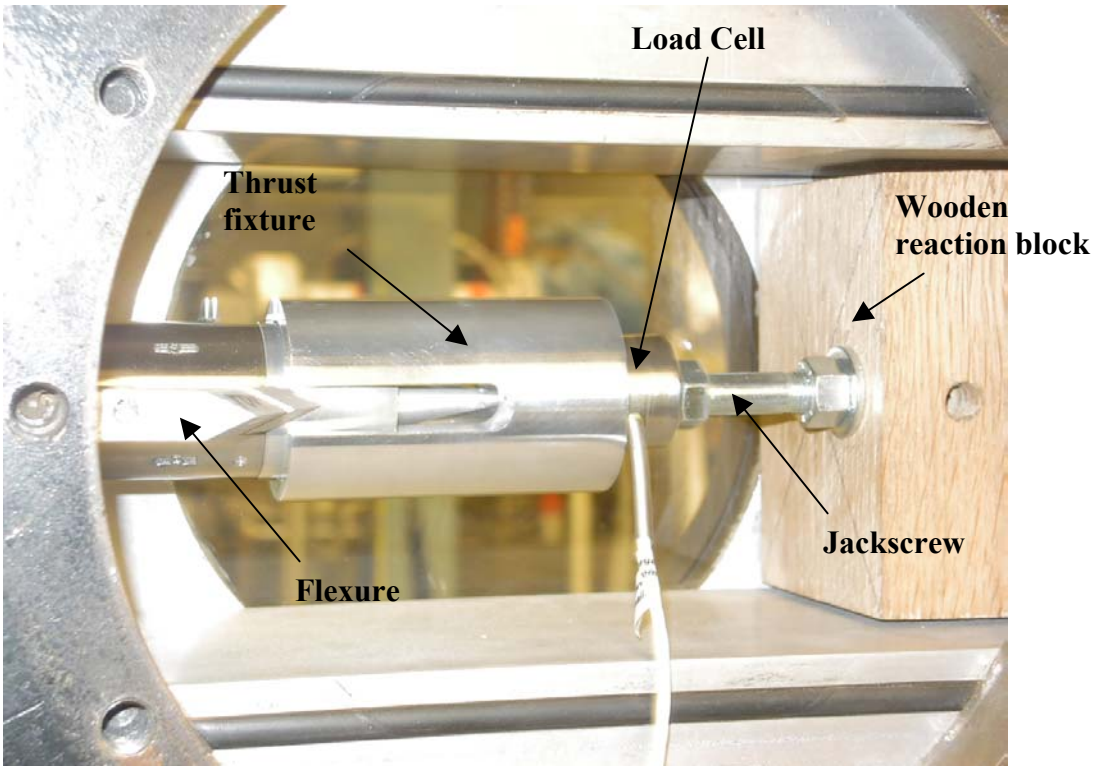

Figure 14. Photograph of the strain-gage calibration setup inside the wind tunnel.

Real time readout of the load cell was displayed on the digital meter. The strain gage outputs were monitored by the DVM on the data acquisition system. The signal conditioning was adjusted at the DAS to produce a value that represented the applied load, which was shown on the digital meter. The applied

force was increased and further adjustment of the read-out on the DAS was carried out. After which the load was fully released, and the zero load voltage read-out noted. Once that was achieved, the calibration set up was dismantled in the reverse order by unscrewing the bolt and nut, followed by removing both the load cell and the thrust collector. Lastly the viewing window for the wind tunnel was installed.

3. Theoretical Drag Prediction

The flow over the ramjet-mounting strut is shown schematically in two dimensions in Figure 15. The flexure was secured with its horizontal axis parallel to the top and bottom walls of the wind tunnel; thus the flexure was at a zero angle-of-attack (AOA). The Mach 4.0 freestream flow would be turned through an angle of 15 degrees by an oblique shock situated at the leading edge. The angle of the oblique shock to the horizontal would be 27.5 degrees. In region 1 shown in Figure 15, the flow Mach number would reduce to 2.8. The flow would then turned back to the horizontal direction through a Prandtl-Meyer expansion fan, which would accelerate the flow to Mach 3.6 in region 2. The flow would then turn toward the trailing edge through a second Prandtl-Meyer expansion fan, which would further accelerate the flow to Mach 4.9 in region 3. The drag force was calculated to be approximately 4.536 lbf for each flexure at zero AOA. Together with the numerical prediction of the drag force induced by the flow on the miniature ramjet [3], the resulting drag force expected was approximately 13.872 lbf in total.

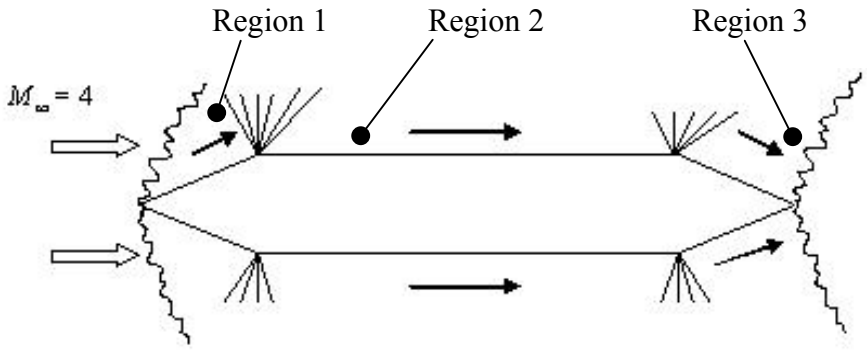

Figure 15. Double modified wedge shock profile.

4. Experimental Drag Measurement and Discussion

Figure 16 shows the measured drag force versus time. Three runs were conducted each over a total time of less than 40 seconds. As can be seen from the plots there was an initial transient load during the starting process of the wind tunnel. The transient lasted the longest (14 seconds) during the first run. In subsequent runs the transient died out faster (6 seconds), however an overshoot of approximately 15% in drag was measured. The sampling time of the data acquisition system was two seconds, thus higher peak values may have been experienced which were not resolved by the DAC system.

One of the attachment points of the flexure arm went through the frame of the window. For each of the runs the initial pre-load in the flexure arm due to closure of the wind tunnel window was measurable. In run 1 the initial pre-load was 0.5 lbf and for runs 2 and 3 the pre-load force was 2 lbf. For each run the steady-state drag force was measured to be 13 lbf above the pre-load. This value was less than that predicted, however the analytical prediction assumed the flow to be two-dimensional over the flexure arms, which was not the case due to the sweep of the arms. Taking sweep into account on the arms would reduce the predicted load to a value less than that measured. The numerical drag predictions [3] did not take the internal struts of the ramjet into account, however it is felt that the contribution to the overall drag of these would be small.

In run 1 there was a slight upward drift of the steady-state drag measurement, which was most probably due to temperature effects during the run. As the length of the run increased these effects became more noticeable, hence they need to be addressed in future testing.

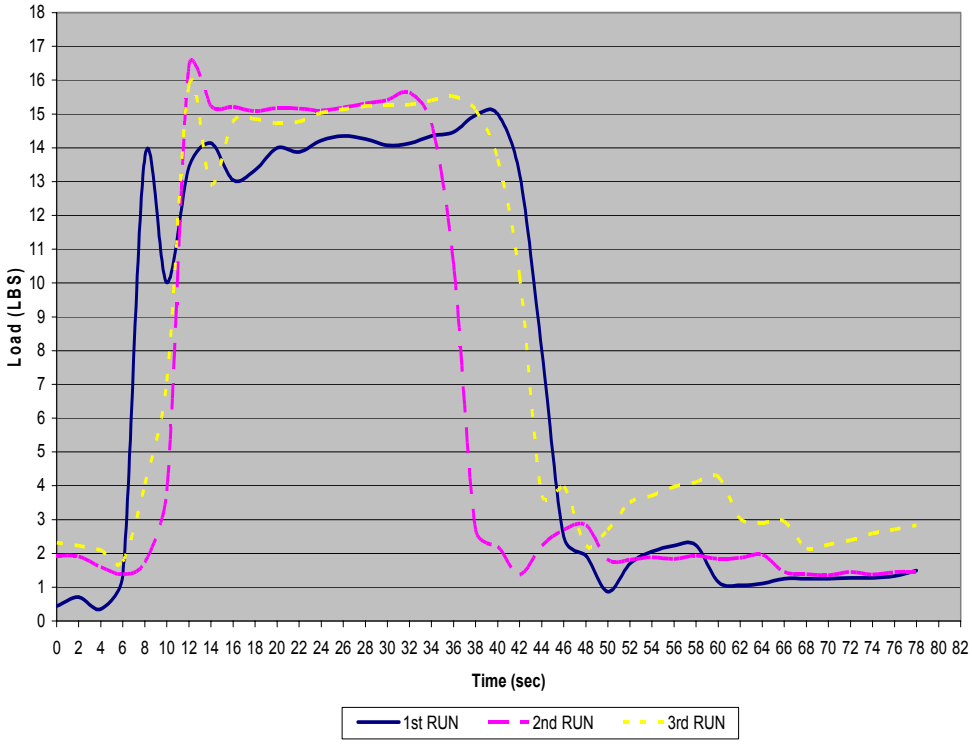

Figure 16. Plot of drag force vs time.

III. NUMERICAL PERFORMANCE PREDICTION

A. METHODLOGY

CFDRC developed a set of computer codes for multi-physics computational analysis. The codes provide an integrated geometry and grid generation module, CFD-GEOM, a graphical user interface for preparation of the model, CFD-GUI, a computational solver for performing the simulation, CFD-ACE(U), and an interactive visualization program for examination and analysis of the simulation results, CFD-VIEW. Although the flow module in CFD-ACE(U) can handle compressible flows, the pressure-based method that CFD-ACE(U) used is not ideally suited to higher supersonic flows. For higher Mach number flows it is better to use a density-based solver like CFD-FASTRAN. This code was developed to simulate and analyze problems dealing with compressible flow, with the additional capability to handle the mixing and combustion of chemical species.

Once the computational domain was defined, it was necessary to ensure that the grid density was sufficient. For most flow problems, the largest gradients will be located near the walls and in free shear layers. Thus it was important to resolve the grid in any location where flow field gradients were expected to be significant.

Combustion dynamics involves coupling between unsteady heat release and pressure oscillations in the combustor. In addition, many parameters that control this process, e.g. fuel injection, fuel-air mixing, shear layer dynamics etc, all involve unsteady processes that interact in a highly non-linear manner. Numerical simulation techniques have to be able to capture this unsteady process in a more realistic manner.

A convergent solution for the fuel-air mixture was obtained prior to the initiation of the combustion model. Figure 17 shows a flow chart for the CFD analysis.

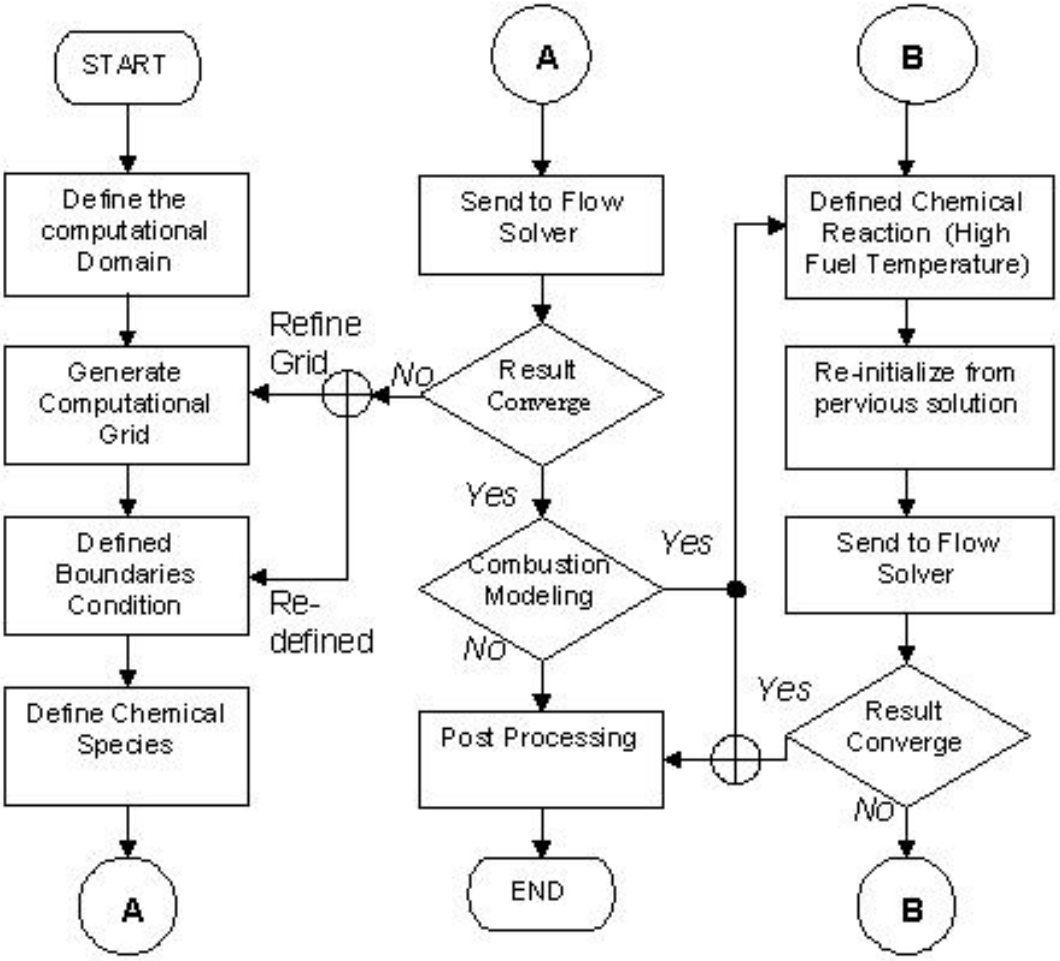

Figure 17. Flow chart for CFD analysis.

To ignite the combustion model, the temperature of the fuel had to be high enough to cause combustion to take place. After the ignition of the combustion, the temperature of the fuel would then be lower to the pre-heat condition to simulate the actual operating condition for the model.

B. TURBULENCE MODEL

In CFD-FASTRAN, a variety of turbulent models are available. In all these models, the effect of turbulence is accounted for via the definition of a turbulent or eddy viscosity. Turbulent models in CFD-FASTRAN are based on Favre-Averaging Navier-Stokes equations that govern the compressible flow physics.

Favre averaging introduces additional terms known as Reynolds stresses. These stresses are modeled using the Boussinesq eddy viscosity concept. Eddy viscosity is not a physical property of the fluid; instead, it is a flow property. Following the kinetic theory of gases, the eddy viscosity is generally modeled as the product of a velocity scale *q* and a length scale *l*. [4]

$$\mu_t = \bar{\rho} q l$$

Various turbulence models differ in the way *q* and *l* are estimated. In CFD FASTRAN, the two-equation models are further divided into high turbulent Reynolds number and low turbulent Reynolds number models. Here high Reynolds number refer to the turbulent Reynolds number,

$$\mathrm{Re}_t = \frac{\rho k^2}{\mu \varepsilon}$$

where *k* is the turbulent kinetic energy and ε is the dissipation rate of turbulence kinetic energy. The $k-\omega$ model is a two-equation model that solves for the transport of ω, the specific dissipation rate of the turbulent kinetic energy, instead of ε. The $k-\omega$ model in CFD-FASTRAN is based on Wilcox [5], which is recast with $\omega = \varepsilon / k$. The eddy viscosity in this model is given by

$$\mu_t = C_\mu \frac{k\rho}{\omega}$$

The transport equations for *k* and ω are

$$\frac{\partial}{\partial t}(\rho k) + \frac{\partial}{\partial x_j}(\rho u_j k) = P - \rho \omega k + \frac{\partial}{\partial x_j}\left[\left(\mu + \frac{\mu_t}{\sigma_k}\right)\frac{\partial k}{\partial x_j}\right]$$

and

$$\frac{\partial}{\partial t}(\rho \omega) + \frac{\partial}{\partial x_j}(\rho u \omega) = C_{\omega_1}\frac{P\omega}{k} - C_{\omega_2}\rho\omega^2 + \frac{\partial}{\partial x_j}\left[\left(\mu + \frac{\mu_t}{\sigma_\omega}\right)\cdot\frac{\partial \omega}{\partial x_j}\right]$$

The model parameters in the above equations are all assigned constant values:

$$C_{\mu} = 0.09 \quad ; \quad C_{\omega_1} = 0.555 \quad ; \quad C_{\omega_2} = 0.833 \quad ; \quad \sigma_k = 2.0 \quad ; \quad \sigma_{\omega} = 2.0$$

This turbulence model was used throughout in order to compare with the numerical results calculated by Ferguson [3]. He also used a $k-\omega$ turbulence model within a NASA code, OVERFLOW, to compute the cold flow through the ramjet at Mach 4.0.

1. Turbulence Flow Quantities

Turbulence intensity for an internal flow can be somewhat large, from 1 to 5%. Throughout this thesis, turbulence intensity was assumed to be 2% [6] of the inlet velocity. The free stream turbulence kinetic energy (k) is calculated using

$$k = \frac{1}{2}\left(u'^2 + v'^2 + w'^2\right)$$

where u' is the turbulent fluctuation velocity, and is equal to the turbulence intensity multiplied by the free stream velocity. The dissipation rate of kinetic energy(ε) and specific dissipation rate of the turbulent kinetic energy (ω) can then be determine from the following equations:

$$\varepsilon = \frac{0.09^{0.75} k^{1.5}}{0.4l}$$

and

$$\omega = \frac{\varepsilon}{k}$$

where l is the length scale. For the purpose of this thesis l was taken as the inlet height. Table 1 shows the turbulence flow quantities used in this thesis with a specific inlet velocity.

Description	Velocity $\left(ft/s\right)$	Length scale (ft)	k $\left(ft^2/s^2\right)$	ε $\left(ft^2/s^3\right)$	ω $\left(1/s\right)$
Inlet	2169	0.1016	2822	184722	65.47
Fuel Injector Port (Strut, 0.02" hole)	328	$5.08x10^{-4}$	64.6	127922	1980.77
Fuel Injector Port (Strut, 0.05" hole)	164	$4.17x10^{-3}$	16	6396	396.15
	246	$4.17x10^{-3}$	36	21586.5	594.23
	328	$4.17x10^{-3}$	64.6	51169	792.3
	410	$4.17x10^{-3}$	101	99939	990.38
Fuel Injector Port (Nose Cone)	413	$4.17x10^{-3}$	103	103558	1002.2
Initial Condition (Nose Cone)	102	$4.17x10^{-3}$	6.2	1524	245.62

Table 1. Turbulence flow quantities used in the model.

C. 2D MODEL SHOCK ANGLE COMPARISON

In order to reduce the computational time required, simulation of a 2D axisymmetric model was carried out to investigate the shock angle, flow field and static temperature and pressure inside the combustion chamber, and compare to results computed by Ferguson [3]. Figure 18, shows the geometry of the 2D axisymmetric model and the computational boundary.

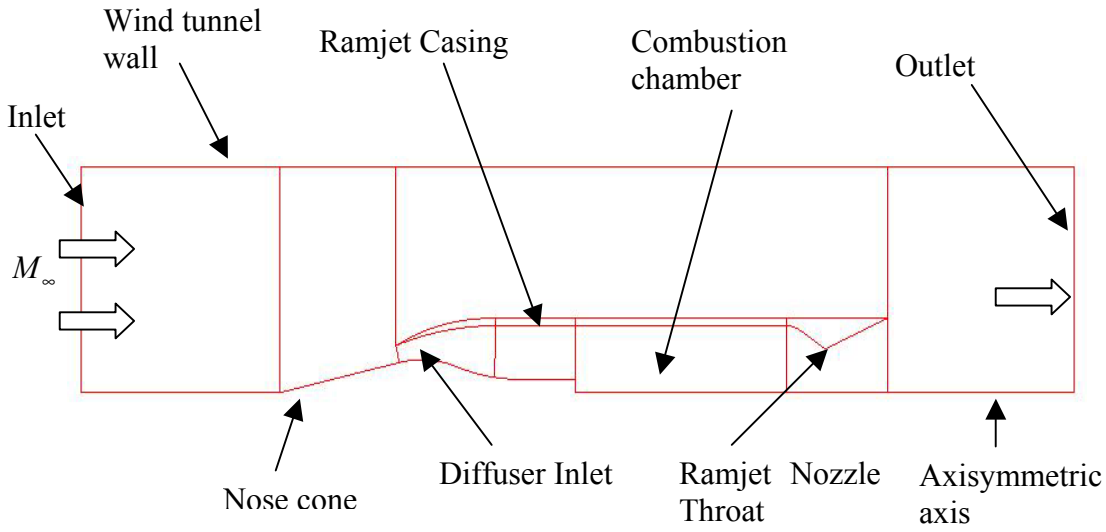

Figure 18. 2D axisymmetric model of ramjet.

1. 2D Grid

A high-density multiblock structured grid with an overall dimension of 376 by 138 was generated using CFD-GEOM. As can be seen in Figure 19, grid clustering was enforced around the leading edge region where significant flow gradients due to shock waves were to be expected.

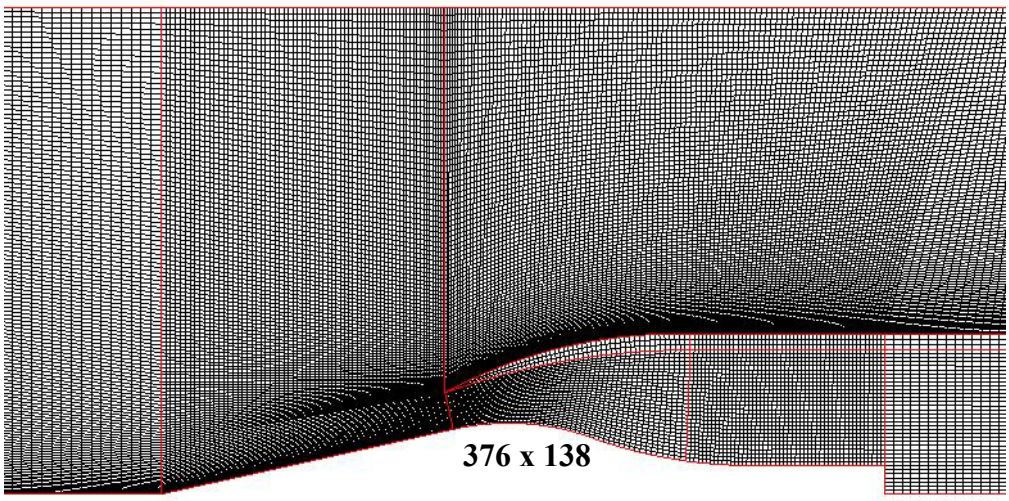

Figure 19. 2D computational grid in the leading edge region.

2. Numerical and Experimental Results and Discussion

Figure 20 shows the computed Mach number distribution through the ramjet at a freestream Mach number of 4.0. The overall distribution and location of the shocks are similar to that predicted by Ferguson [3] as shown in Figure 21. Figure 20 also indicated that the flow after the oblique shock was reduced to about Mach 3. The flow after the second shock reduced drastically to around Mach 0.3 which was the ideal flow speed inside the combustion chamber.

The numerical result surprisingly did not produce a normal shock. Instead, it shows what looks more like an oblique shock after the lip of the diffuser inlet. This phenomenon was also observed in Ferguson's [3] prediction. It could be due to a few factors; higher grid density is required at the diffuser inlet, the nose cone angle is not optimized, and the nozzle throat diameter is not optimized. Figure 20 also shows the reflection of the shock wave against the wind tunnel wall, whereas the solution in Figure 21 did not develop such phenomenon. This is mainly because the wind tunnel wall is not being modeled as part of the boundary conditions in Ferguson's [3] simulation.

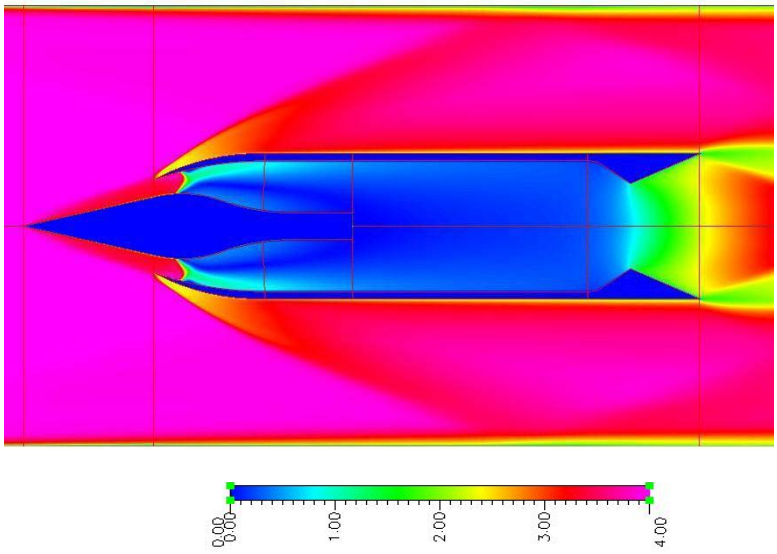

Figure 20. 2D numerical shock profile prediction using CFDRC-FASTRAN.

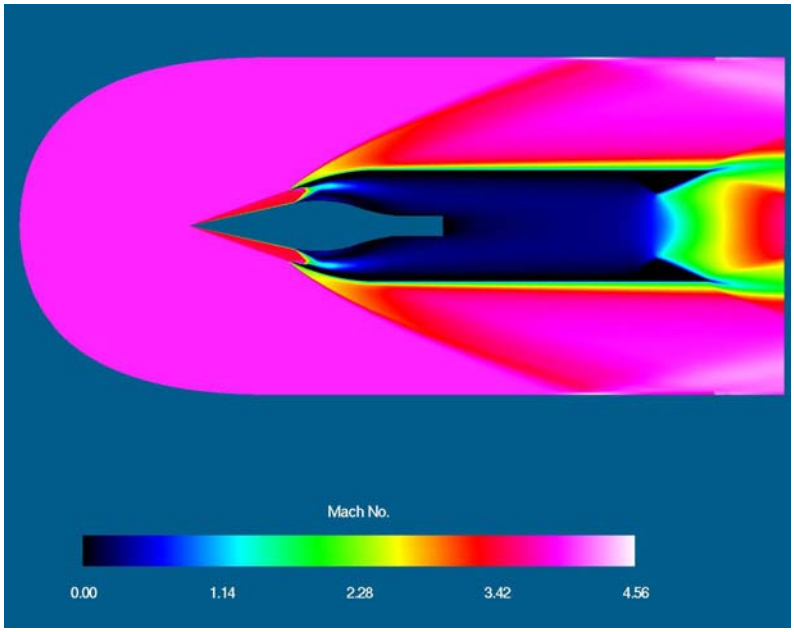

Figure 21. 2D numerical shock profile prediction using Overflow code.

The numerical prediction and the experimental shock profiles were very similar, with both indicating that the oblique shock did not sit at the lip of the diffuser inlet. Figure 22 shows the details of the numerically predicted external shock structure. Figure 23 shows a shadowgraph image of the shock profile taken during the cold flow Mach 4 wind tunnel testing.

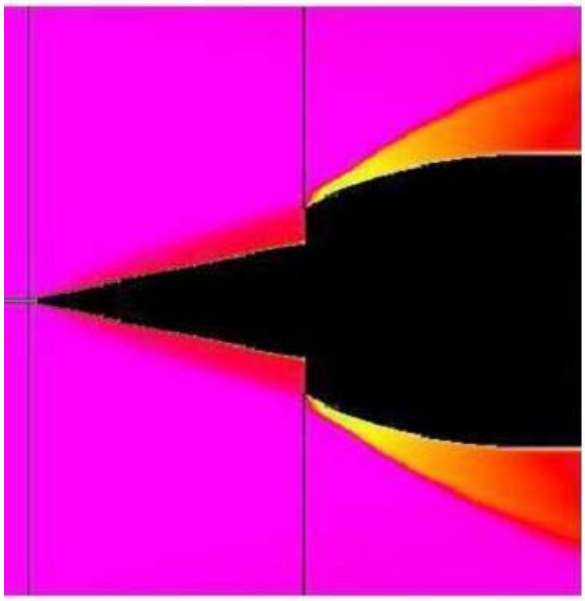

Figure 22. 2D numerical shock profile prediction for Mach 4 flow analysis.

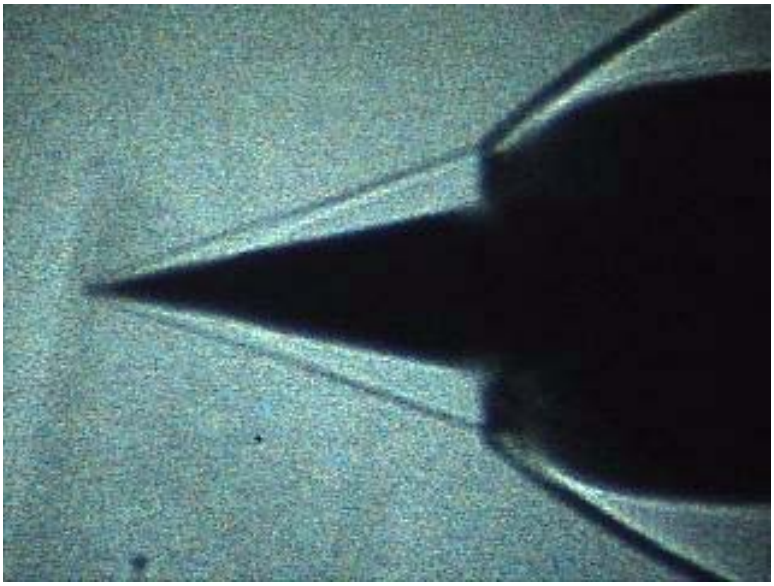

Figure 23. A shadowgraph image of the shock profile at Mach 4.

The 2D simulation results also indicated that the ramjet design had a pressure recovery ratio of about 13.6 with an average chamber pressure of 14.5 psia (1 bar). Figure 24 shows the pressure distribution inside the ramjet with the flow field pressure of 1.07 psia (7378 Pa).

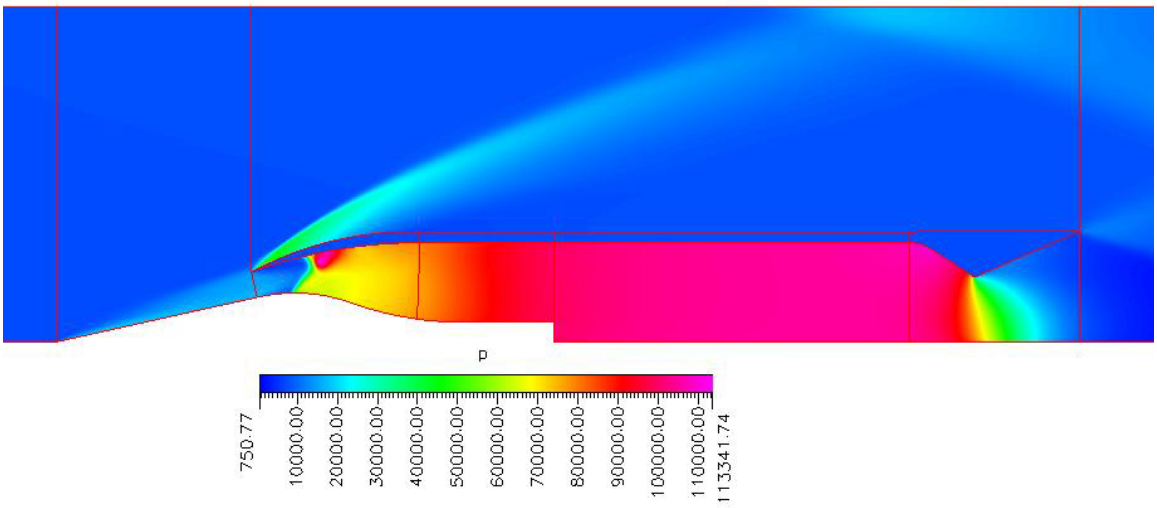

Figure 24. 2D pressure distribution profile for Mach 4 flow analysis (note pressure in Pa)

The design also provided a temperature recovery ratio of about 4.4 with an average chamber temperature of 80°F (300 K). Figure 25 shows the temperature distribution, with the flow field temperature of -337.3°F (68 K).

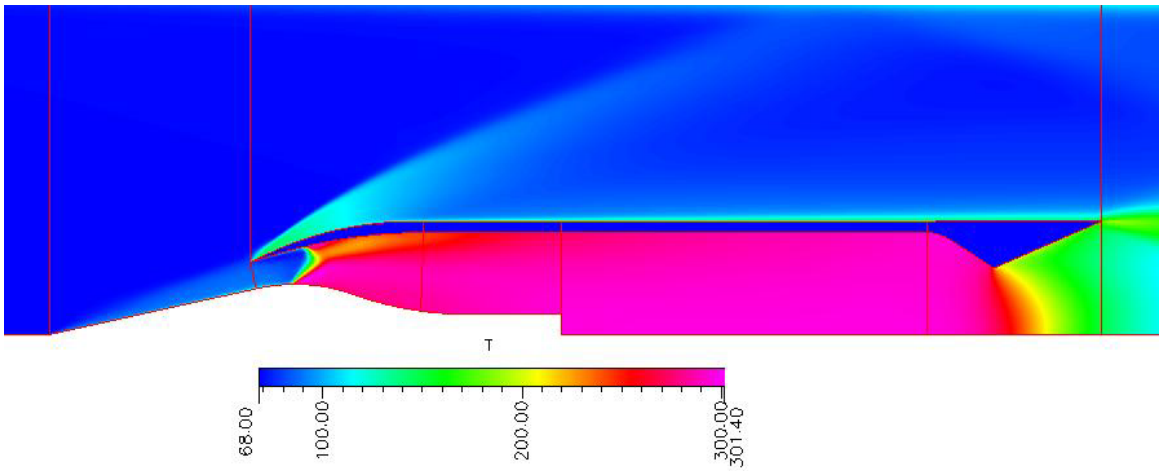

Figure 25. 2D temperature distribution profile of Mach 4 flow analysis (note temperature in Kelvin).

D. 3D FUEL-AIR MIXTURE ANALYSIS

Fuel-air mixing was numerically predicted under a variety of injection conditions. The impact of the flow on the state of mixing was also investigated. The numerical complexity of a 3D model would require huge computational times as well as large memory space. In order to model the problem with reduced computational time and memory, a 45 degree slice of the actual model was created as shown in Figure 26. Two symmetric planes were used in this model, with one cutting across the centre of the strut and the other slicing across the center axis of the nose injection port. The internal wall of the wind tunnel was not modeled, since the focus for the fuel mixing was from the tip of the nose cone and from the strut to the combustion chamber inside the ramjet.

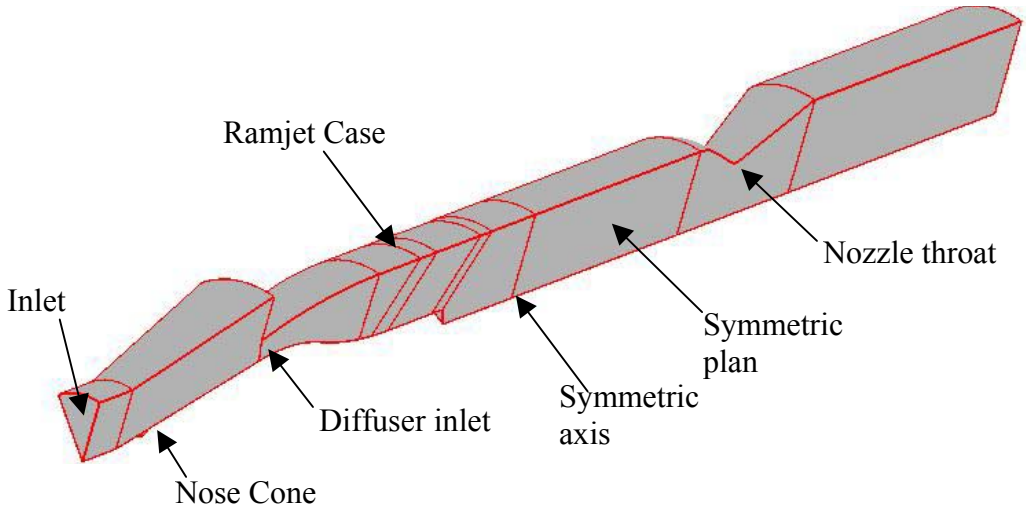

Figure 26. 3D geometry of the model formed by multiple blocks.

1. 3D Grid

Structured grids were once again used in the model. Multi-block methods were used to process multiple structured grids, which formed the entire numerical domain. The interface between two structured grid blocks must have a one-to-one match on the number of grids. This mean that each face in one grid must be aligned with the other one face in an adjacent grid. A total of twelve structured grid blocks were used to create the model, and the overall grid dimensions were 15 x 387 x 51 with 183190 cells in total. Figure 27 shows an overall picture of the grid density used to create the computational domain for the ramjet model. Figures 28 and 29 show a close-up view of the grids distribution on the nose cone and on the internal strut respectively.

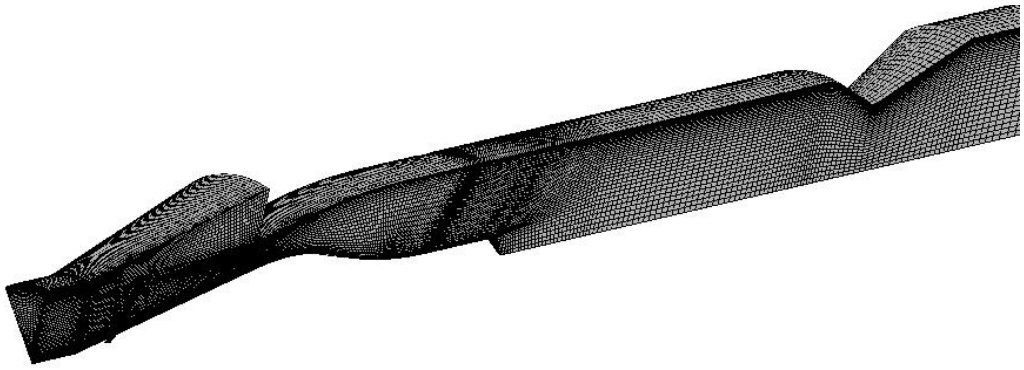

Figure 27. Pictures of a 3D grid profile for the entire computational domain.

The fuel injection ports were modeled as square patches, as this simplified the grid generation. However, the cross-sectional area of the port as designed and manufactured was initially simulated. In subsequent simulations the port area was increased by 5 times.

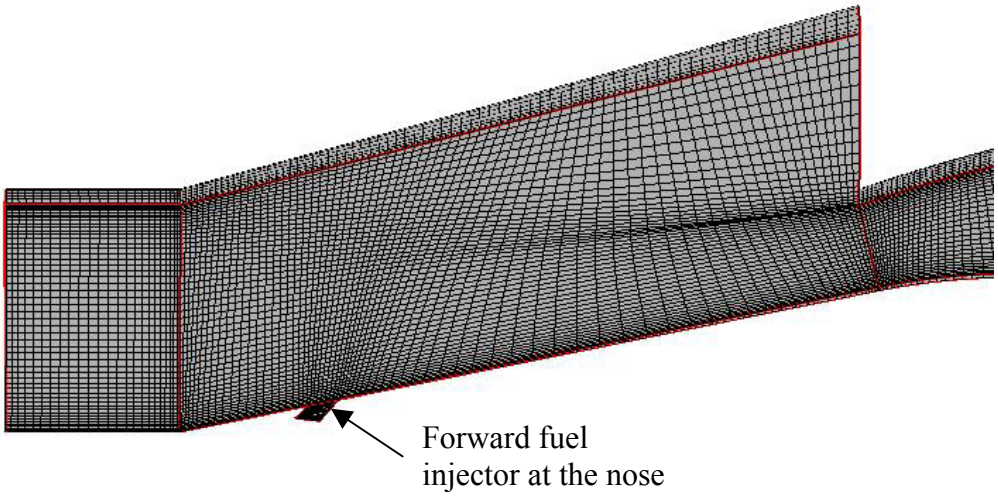

Figure 28. Picture of the grid density used in the forward section of the model.

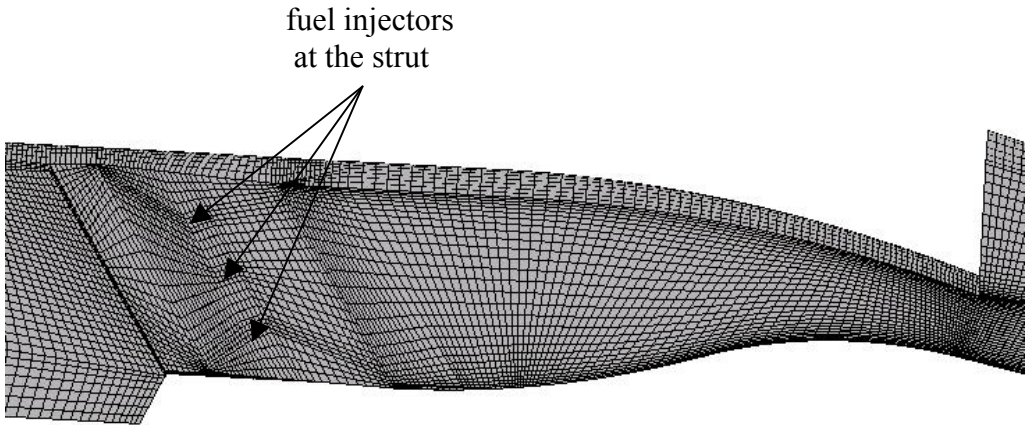

Figure 29. Picture of the grid density used for the 3 fuel injection ports at the strut.

2. Flow Parameter

A simple air model containing 76.8% nitrogen and 23.2% oxygen was assumed and used through out the simulation. The fuel used was propane, C_3H_8, which too was used through out the simulation.

Figure 30 shows the axial length verses the radial height of the 3D model. The combustion chamber is located at an axial position between 0.08” to 0.13”. While the fuel injection ports on the strut are located at an axial length of approximately 0.07” and the fuel injection port at the nose is located at an axial length of approximately 0.006”.

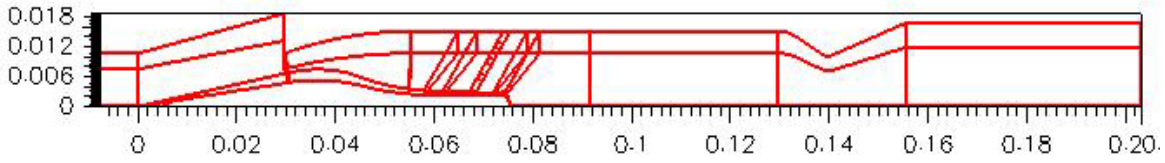

Figure 30. Axial length vs radial height of the model.

Based on the required fuel consumption of 0.019 lbm/s and the captured air flow of 0.096 lbm/s, as determined using GASTURB [3], the required fuel-air ratio was determined to be about 0.2, which was equivalent to 1 part of fuel to 5 parts of air. Since there were six fuel injectors of $0.02"$ diameter in each strut, It was determined that the fuel injection velocity of 2913 ft/s (888 m/s) would be needed to provide the required fuel mass flow rate. This assumed that the fuel was gaseous and had a density of approximately 0.12 lbm/ft^3. It was determined that a total of 24 fuel injection ports of $0.0596"$ diameter would be required to provide the mass flow rate, with each injector providing a more reasonable injection velocity of 328 ft/s (100 m/s), based on a fuel temperature of 80 $^\circ F$ (300 K).

3. Data Collection Reference Point

Two “probe lines” were used through out the analysis to compare the simulation results taken across the length (chord) of the model. As shown in Figure 31, one of the points was measured at 0.0006 inches away from the center injector on the strut while the second point was taken at the symmetric plane in line with the center of the nose injector.

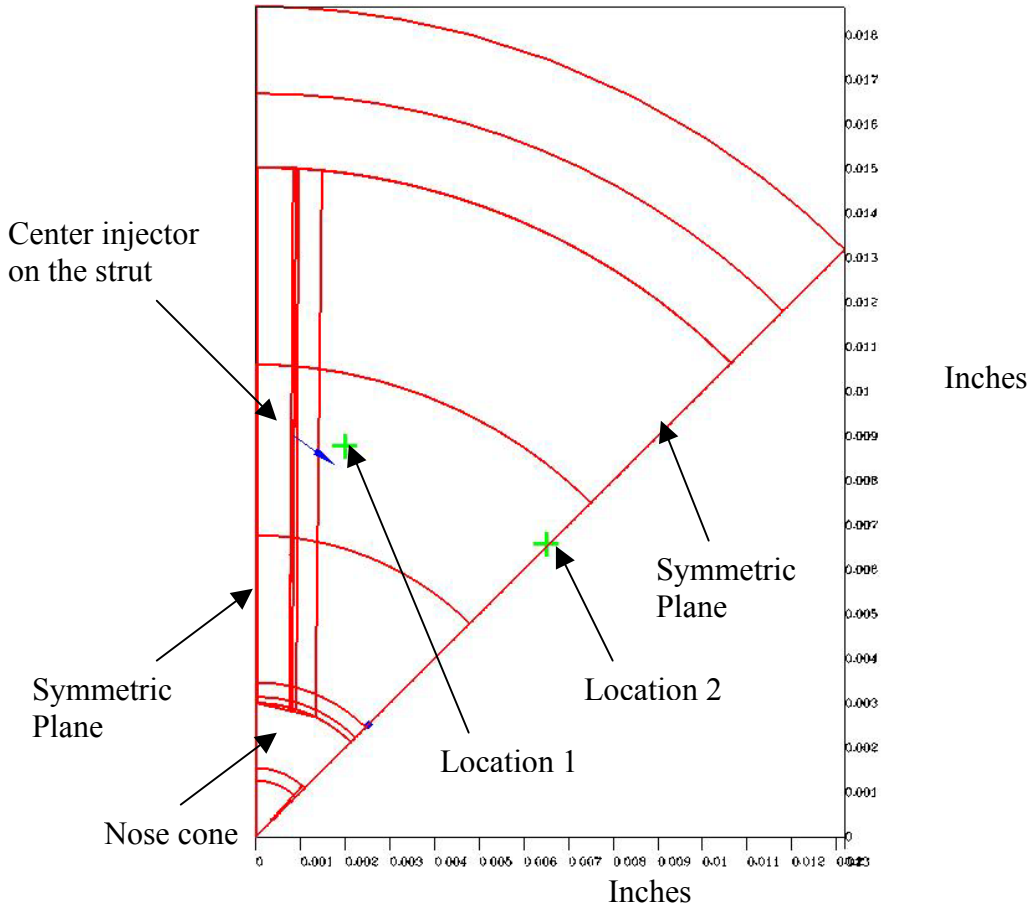

Figure 31. Showing the measuring locations where numerical data were collected.

4. Results and Discussion

Table 2 shows a tabulated list of the propane mass fraction with various injection velocities, based on a fuel temperature of $80^{\circ}F$ (300 K), measured at the axial location of 0.1 chord length on the two locations, as show in Figure 31.

Injection Velocity $\left(ft/s\right)$	Location 1 0.05” holes	Location 2 0.05” holes	Location 1 0.02” holes	Location 2 0.02” holes
164	0.057	0.04	0.0086	0.006
246	0.085	0.051	-	-
328	0.125	0.056	-	-
410	0.146	0.0942	-	-

Table 2. Propane mass fraction prediction at 0.1 axial length.

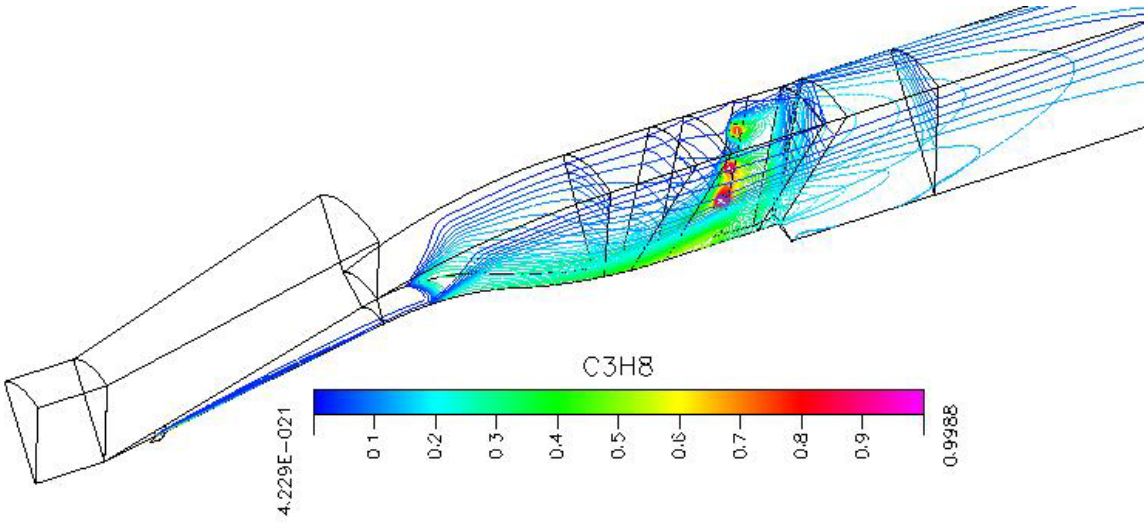

Figure 32. Predicted propane concentration at Mach 4 free-stream condition.

The simulation results indicate that with an enlargement of about 2.5 times the original design fuel injection port diameter on the strut would increase the fuel concentration by a factor of approximately 7 as indicated in Table 2, using the 164 ft/s (50 m/s) injection velocity.

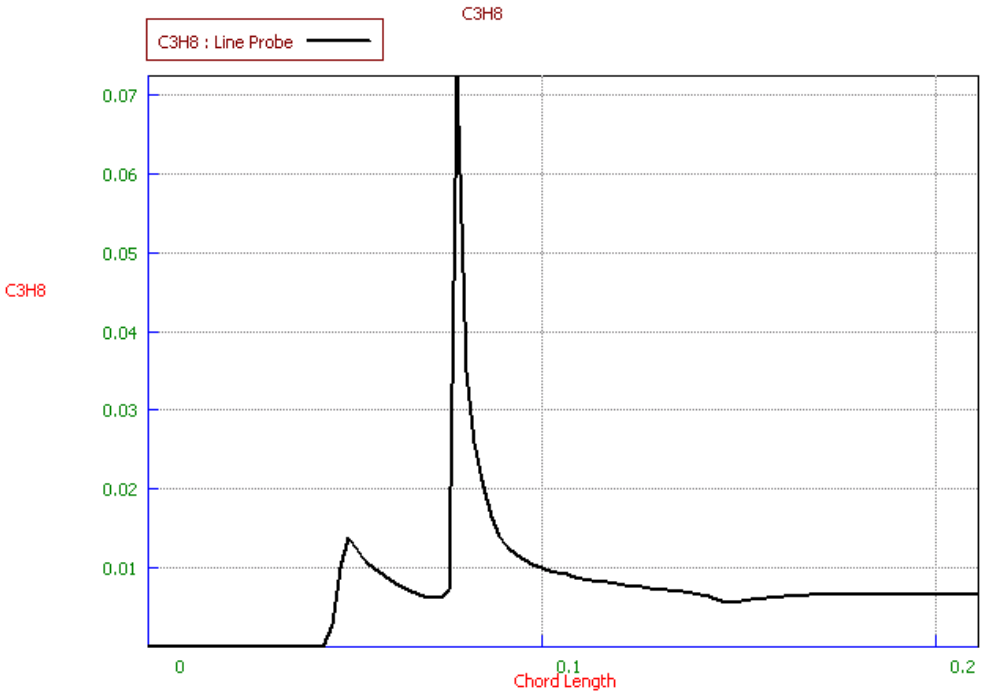

Figure 33. Plot of propane concentration vs chord length for a 0.02” hole with 164ft/s flow rate measured at location 1.

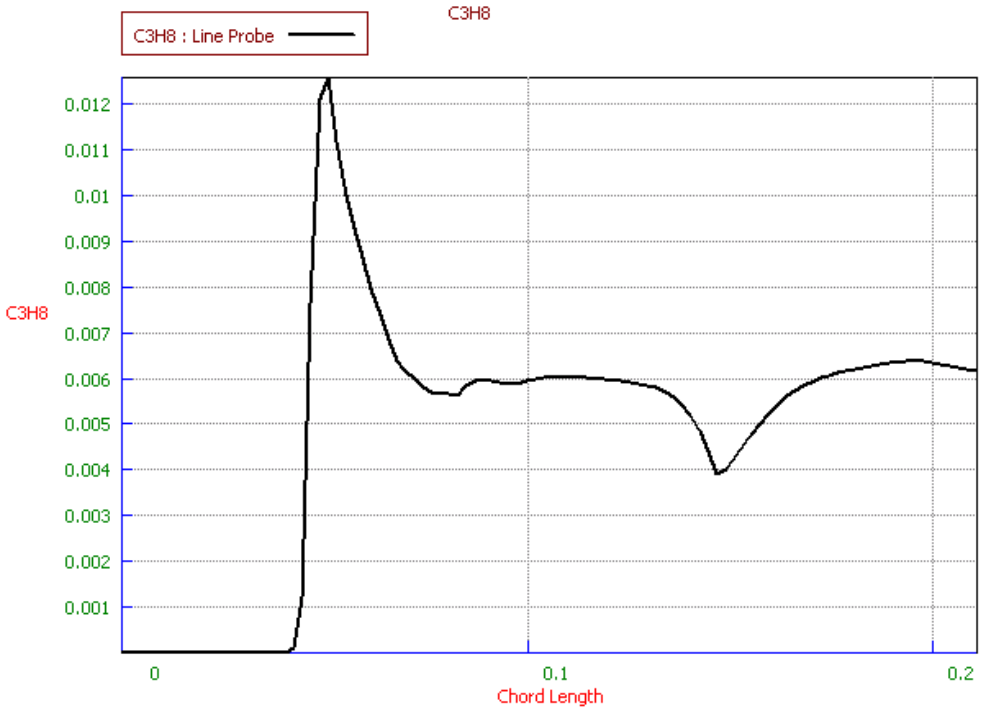

Figure 34. Plot of propane concentration vs chord length for a 0.02” hole with 164ft/s flow rate measured at location 2.

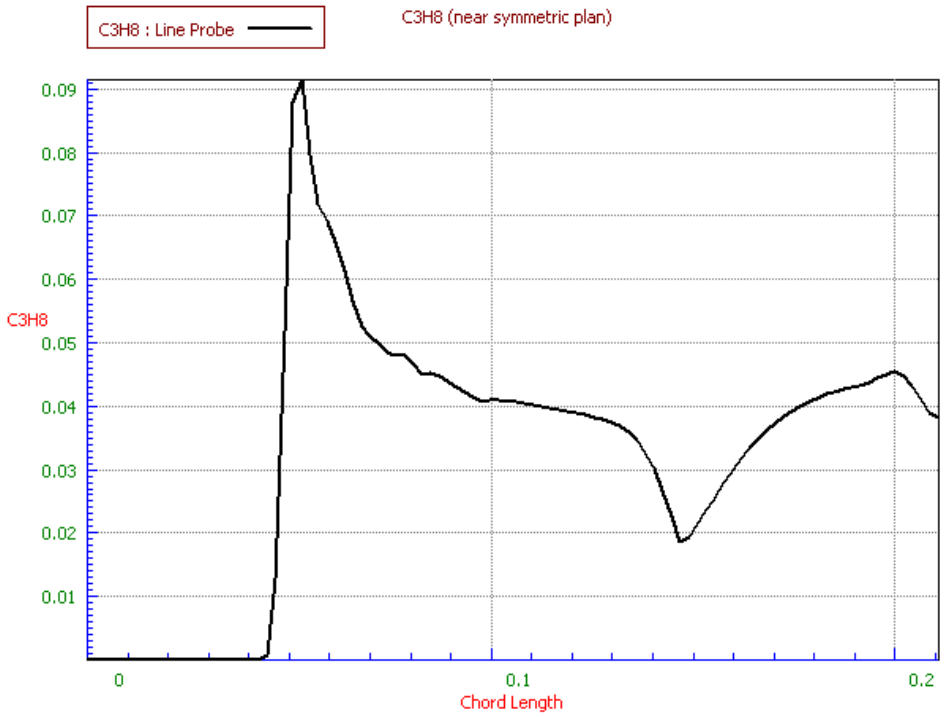

Figure 35. Plot of propane concentration vs chord length for a 0.05” hole with 164ft/s flow rate measured at location 1.

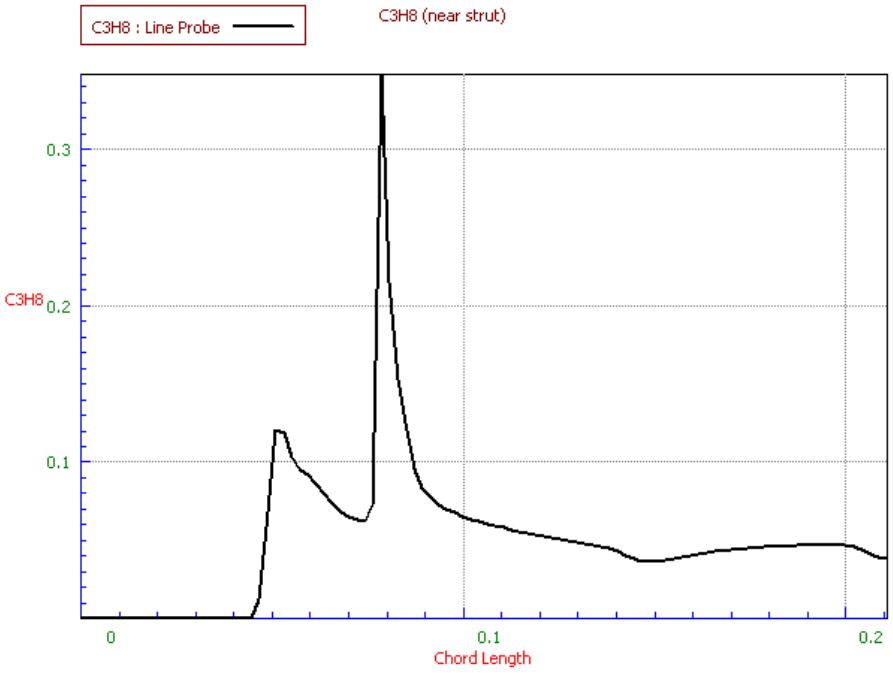

Figure 36. Plot of propane concentration vs chord length for a 0.05” hole with 164ft/s flow rate measured at location 2.

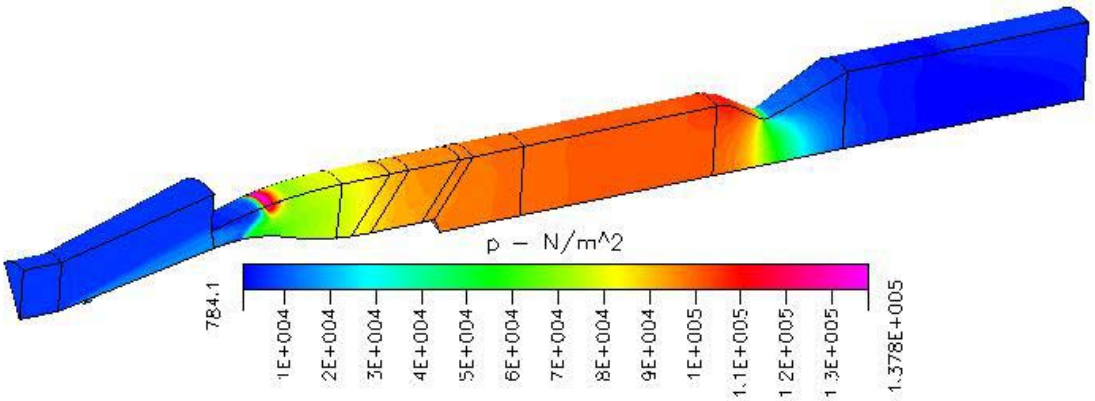

Figure 37. Picture of pressure distribution with fuel mixing analysis.

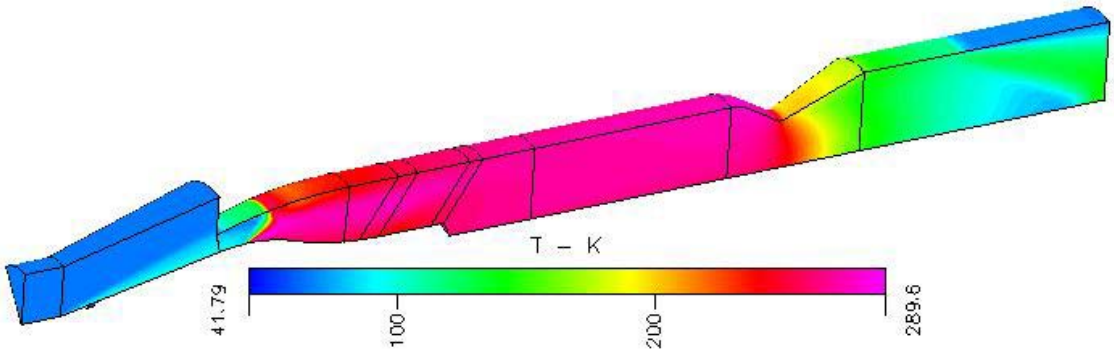

Figure 38. Picture of temperature distribution with fuel mixing analysis.

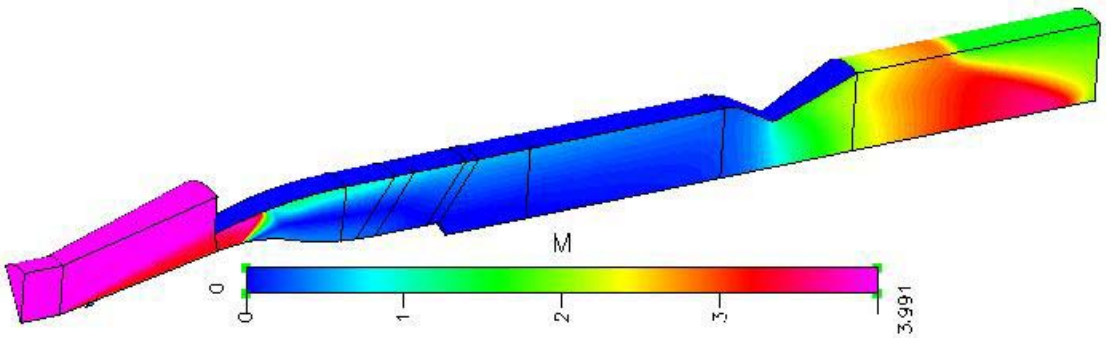

Figure 39. Plot of Mach number vs axial length with fuel mixing analysis.

Figure 37 shows the pressure distribution within the computational domain. The pressure recovery ratio of approximately 15 was predicted with the chamber pressure of about 15.95 psia (110 kPa) and a flow field pressure of 1.07 psia (7378 Pa). This was an increase of about 11% as compared to the 2D model, without the additional of fuel, as shown in Figure 24.

Figure 38 shows the temperature distribution within the computational domain. The temperature recovery ratio was about 4 with an average chamber temperature of approximately 26$^{\circ}F$ (270K) and the flow field temperature of -337.3$^{\circ}F$ (68K). This was a reduction of about 9% from the 2D result, without the introduction fuel mixing, as shown in Figure 25.

Figure 39 shows the picture of the Mach number distribution within the computational domain. The Mach number within the combustion chamber was about 0.3 for both results, with or without the introduction of the fuel.

E. COMBUSTION ANALYSIS

The CFD-ACE flow solver only supported finite rate chemistry for combustion analysis with species mass fraction predicted. The finite rate (species fraction approach) model allowed the specification of a single or multi-step irreversible or reversible chemical reaction, which proceeded at a finite rate to completion. This mechanism can only be used with the species mass fraction approach. For reacting gases, the governing equations for mass are based on each chemical species in the domain. The reaction terms act as source terms for the species equations. [7]

Two step reaction mechanisms were used in the model. The two reaction equations are

$$C3H8 + 3.5O_2 \Leftrightarrow 3CO + 4H_2O$$ ---------- Reaction 1

and

$$CO + 0.5O_2 \Leftrightarrow CO_2$$ ---------- Reaction 2

The model assumed that the rate coefficients to have an Arrhenius form;

$$k_f = AT^n e^{\left(-E_a/RT\right)}$$

where

k_f = reaction rate coefficient

A = pre-exponential constant

n = temperature exponent

E_a/R = activation temperature

Reaction Parameter	Forward Reaction 1	Backward Reaction 1	Forward Reaction 2	Backward Reaction 2
A	5.623E+09	0	2.239E+12	2.121E+17
n	0	0	0	-0.5
P	0	0	0	0
E/R	15100	0	20140	53800

Table 3. Finite rate reaction quantities used in the combustion model.

Reaction Parameter	Forward Reaction 1	Backward Reaction 1	Forward Reaction 2	Backward Reaction 2
$C3H8$	0.1	-	-	-
O_2	1.65	-	0.5	-
CO	-	1	1	-
H_2O	-	1	-	-
CO_2	-	-	-	1

Table 4. Species concentration exponents.

1. Result and Discussion

Combustion modeling was only successful with a two-dimensional model using CFD-ACE with a very low inlet velocity of 15 m/s. No sustained combustion could be achieved with FASTRAN and high supersonic inlet flow.

Figure 40 shows the temperature distribution inside the combustion chamber prior to the fuel ignition. The fuel was injected at 1880$^{\circ}F$ (1300K) initially to simulate preheating prior to combustion. The temperature diffused rapidly as the hot fuel was injected into the combustion chamber.

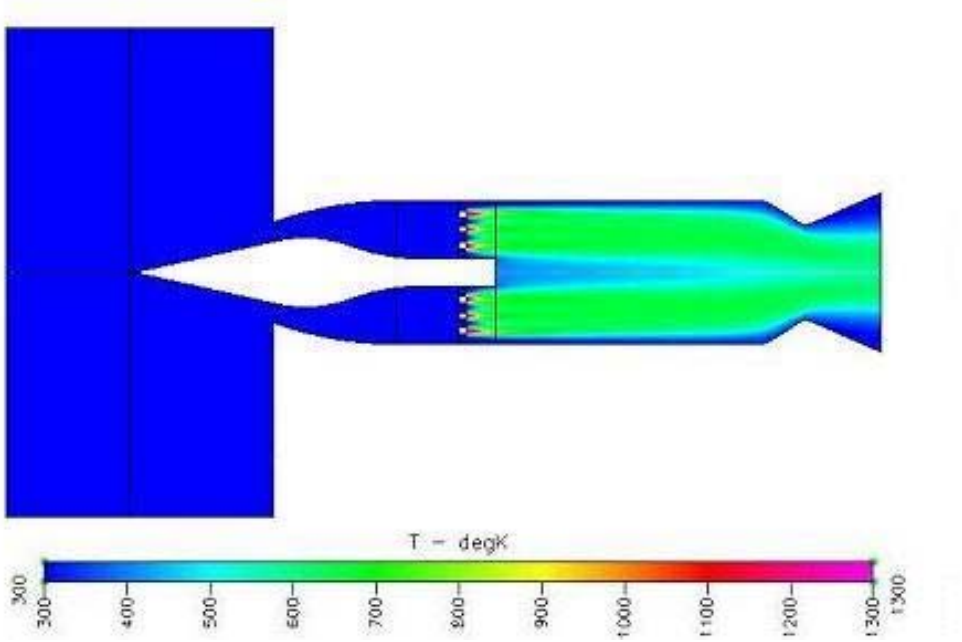

Figure 40. Temperature distribution inside the combustion chamber prior to ignition (note temp. in Kelvin).

Figure 41 shows the combustion temperature inside the combustion chamber after ignition. The predicted combustion temperature was between 4040$^{\circ}F$ (2500K) to 5840$^{\circ}F$ (3500K). The temperature closer to the strut injection port was between 2240$^{\circ}F$ (1500K) to 3140$^{\circ}F$ (2000K). The temperature at the nozzle throat rose to about 6740$^{\circ}F$ (4000K). Figure 42 shows the concentration of carbon monoxide (CO) in the combustion chamber.

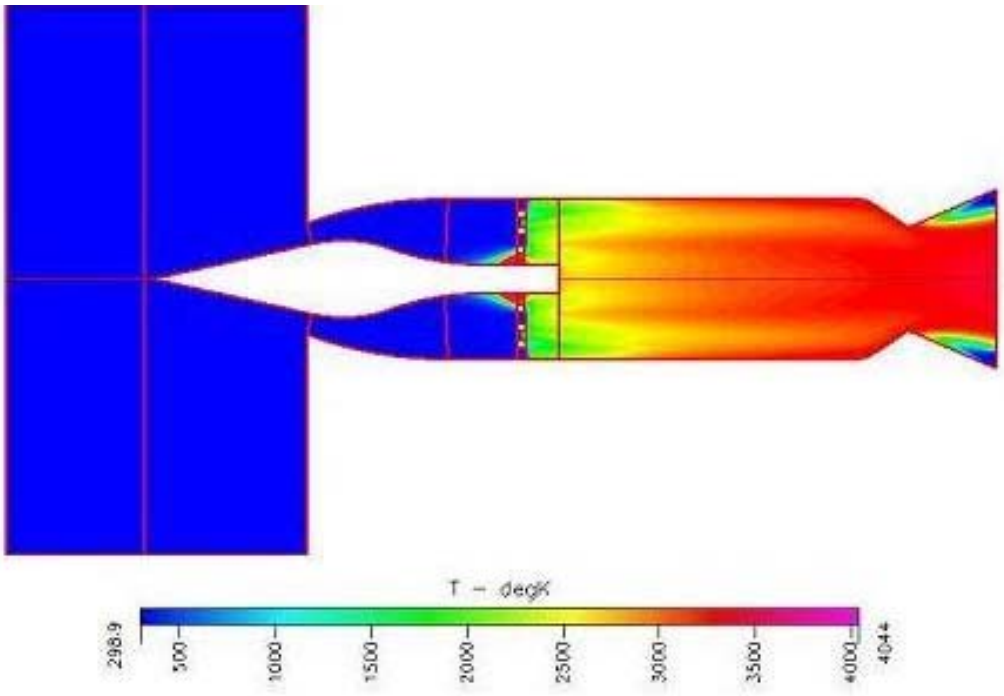

Figure 41. Temperature distribution inside the combustion chamber during combustion (note temp. in Kelvin).

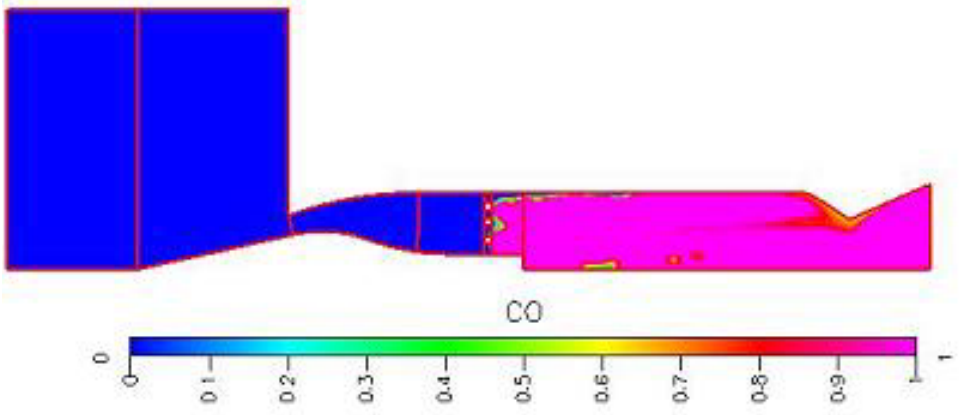

Figure 42. CO concentration during combustion analysis.

IV. CONCLUSION AND RECOMMENDATIONS

The drag on the miniature ramjet in the Mach 4 wind tunnel was successfully measured to be about 13 lbf. This was done by instrumentation of the flexure arms, which held the ramjet model in place in the 4" x 4" test section. The prediction by both CFD and analytically of drag on the model, compared well with the experimental results.

The two-dimensional (axis-symmetric) simulation of the ramjet in a Mach 4 flow without combustion with CFD-FASTRAN compared well with previous predictions performed with a NASA code. Three-dimensional, axi-symmetric modeling of a 45° slice through the ramjet was also successfully carried out. The 3D model included the simulation of the internal struts within the ramjet as well as the fuel injection ports on the struts and close to the tips of the nose cone. The model also included the introduction of gaseous propane through the injector and thus the fuel concentration ratios were predicted at Mach 4 free stream conditions. The current diameter of the injection ports was not sufficient to support the required fuel-air ratio of 0.2. A 2.5 times increased in the injection port diameter would be needed to increased the fuel concentration by a factor of 7.

A subsonic two-dimensional model, including combustion, of the strut-delivered propane was successfully completed. The preheated fuel 1340°F (1000K) and air mixture was run to convergence before combustion was initiated in the numerical model. A combustion chamber temperature of 4940°F (3000K) was predicted.

THIS PAGE INTENTIONALLY LEFT BLANK

APPENDIX A. STRAIN GAGE

When a metal filament is expanded or contracted due to external force, it experiences a change in it's electrical resistance. By bonding a metal filament onto the surface of a test article, the metal will change it's shape according to the expansion or contraction of the test article, thus resulting in a change in its resistance. A strain gage is a form of sensor making use of the changes in resistance to detect the strain induced in a test article under stress. A strain gage is constructed by bonding a fine electric resistance wire to an electrical insulation base, and attaching gage leads. Strain gages are bonded on to the surface of the test article with specified adhesives. The strain generated in the test article is transmitted to the resistor through the gage base, where expansion or contraction occurs. As a result, the resistor experiences a variation in resistance. Careful selection of the strain gage would be required so as to optimize the gage performance under a specified environmental and operating condition. Obtaining strain measurement that was accurate and reliable at the same time was the goal. However the complexity of the installation needed to be controlled so as to minimize the total cost of the entire gage installation. The maximum expected strain value as determined by the simulation result, and the temperature that the gage would see, were the key factors for the selection of the CEA series strain gage. [See Appendix B for the Data Sheet]. Figure 43 shows a typical strain gage layout.

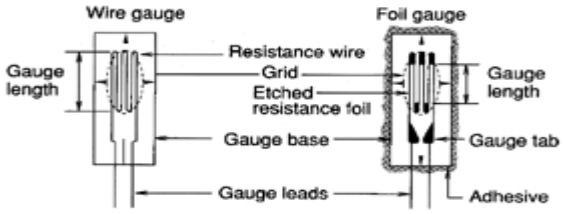

Figure 43. Typical Strain gage.

THIS PAGE INTENTIONALLY LEFT BLANK

APPENDIX B. STRAIN GAGE DATA SHEET

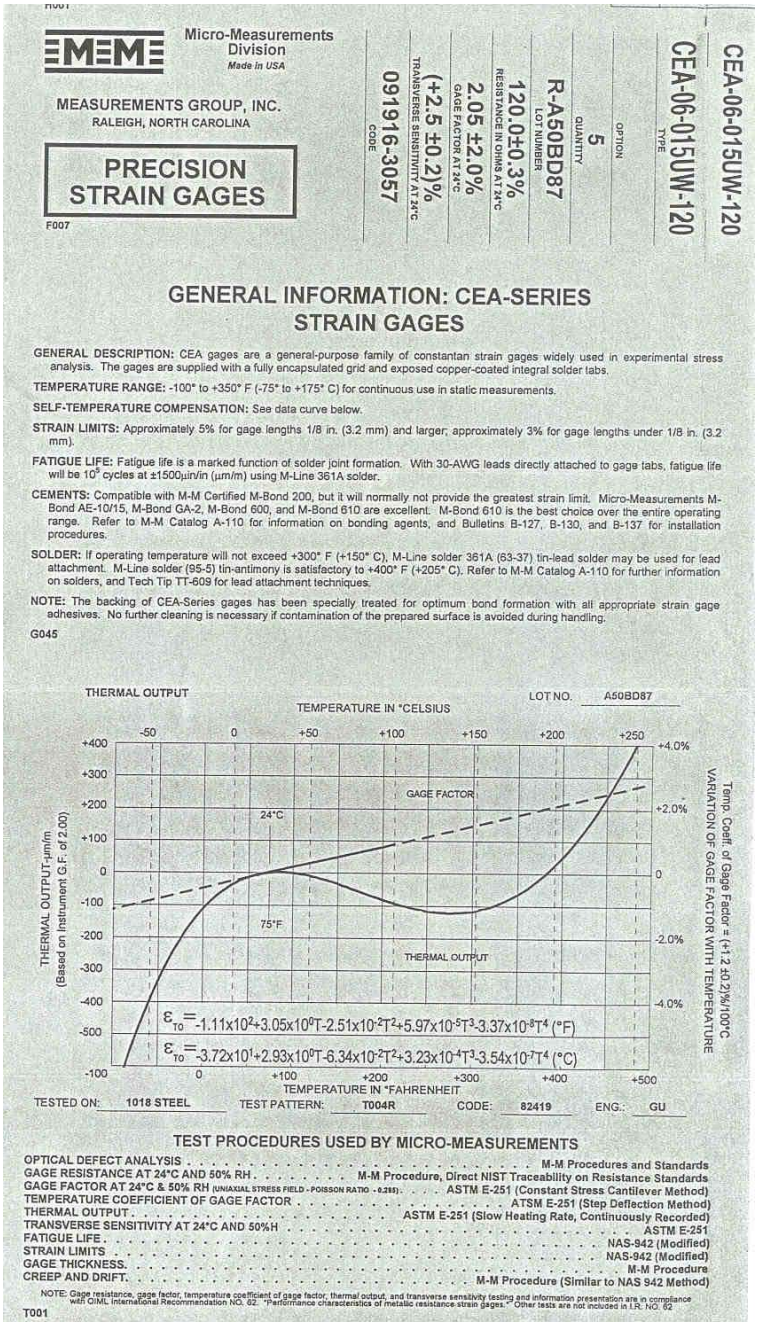

Micro-Measurements Division
Made in USA

MEASUREMENTS GROUP, INC.
RALEIGH, NORTH CAROLINA

PRECISION STRAIN GAGES

F007

CEA-06-015UW-120

TYPE: CEA-06-015UW-120
OPTION:
QUANTITY: 5
LOT NUMBER: R-A50BD87
RESISTANCE IN OHMS AT 24°C: 120.0±0.3%
GAGE FACTOR AT 24°C: 2.05 ±2.0%
TRANSVERSE SENSITIVITY AT 24°C: (+2.5 ±0.2)%
CODE: 091916-3057

GENERAL INFORMATION: CEA-SERIES STRAIN GAGES

GENERAL DESCRIPTION: CEA gages are a general-purpose family of constantan strain gages widely used in experimental stress analysis. The gages are supplied with a fully encapsulated grid and exposed copper-coated integral solder tabs.

TEMPERATURE RANGE: -100° to +350° F (-75° to +175° C) for continuous use in static measurements.

SELF-TEMPERATURE COMPENSATION: See data curve below.

STRAIN LIMITS: Approximately 5% for gage lengths 1/8 in. (3.2 mm) and larger; approximately 3% for gage lengths under 1/8 in. (3.2 mm).

FATIGUE LIFE: Fatigue life is a marked function of solder joint formation. With 30-AWG leads directly attached to gage tabs, fatigue life will be 10^6 cycles at ±1500μin/in (μm/m) using M-Line 361A solder.

CEMENTS: Compatible with M-M Certified M-Bond 200, but it will normally not provide the greatest strain limit. Micro-Measurements M-Bond AE-10/15, M-Bond GA-2, M-Bond 600, and M-Bond 610 are excellent. M-Bond 610 is the best choice over the entire operating range. Refer to M-M Catalog A-110 for information on bonding agents, and Bulletins B-127, B-130, and B-137 for installation procedures.

SOLDER: If operating temperature will not exceed +300° F (+150° C), M-Line solder 361A (63-37) tin-lead solder may be used for lead attachment. M-Line solder (95-5) tin-antimony is satisfactory to +400° F (+205° C). Refer to M-M Catalog A-110 for further information on solders, and Tech Tip TT-609 for lead attachment techniques.

NOTE: The backing of CEA-Series gages has been specially treated for optimum bond formation with all appropriate strain gage adhesives. No further cleaning is necessary if contamination of the prepared surface is avoided during handling.

G045

TEST PROCEDURES USED BY MICRO-MEASUREMENTS

OPTICAL DEFECT ANALYSIS	M-M Procedures and Standards
GAGE RESISTANCE AT 24°C AND 50% RH	M-M Procedure, Direct NIST Traceability on Resistance Standards
GAGE FACTOR AT 24°C & 50% RH (UNIAXIAL STRESS FIELD - POISSON RATIO - 0.285)	ASTM E-251 (Constant Stress Cantilever Method)
TEMPERATURE COEFFICIENT OF GAGE FACTOR	ATSM E-251 (Step Deflection Method)
THERMAL OUTPUT	ASTM E-251 (Slow Heating Rate, Continuously Recorded)
TRANSVERSE SENSITIVITY AT 24°C AND 50%H	ASTM E-251
FATIGUE LIFE	NAS-942 (Modified)
STRAIN LIMITS	NAS-942 (Modified)
GAGE THICKNESS	M-M Procedure
CREEP AND DRIFT	M-M Procedure (Similar to NAS 942 Method)

NOTE: Gage resistance, gage factor, temperature coefficient of gage factor, thermal output, and transverse sensitivity testing and information presentation are in compliance with OIML International Recommendation NO. 62. "Performance characteristics of metallic resistance strain gages." Other tests are not included in I.R. NO. 62

T001

Figure 44. Strain gage data sheet.

THIS PAGE INTENTIONALLY LEFT BLANK

APPENDIX C. WHEATSTONE BRIDGE

Resistance of a strain gage changes proportionally to the received strain. Strain is measured by measuring this resistance change. Since the resistance change is very small in most cases, it requires a Wheatstone bridge circuit to convert the small resistance change into measurable voltage output. An input DC voltage, or excitation voltage, is applied across the top and bottom of the bridge circuit, and the output voltage is measured across the middle. When the output voltage is zero, the bridge is balanced. A changed in the resistance for one of the strain gages would cause the previously balanced bridge to be unbalanced. This unbalance results in an induced voltage appearies across the middle of the bridge. This induced voltage may be measured with a voltmeter. In either case, the change in resistance that caused the induced voltage may be measured and converted to obtain an engineering unit, using a digital or analog data acquisition system. The full bridge method was used in the present study, as shown in Figure 45.

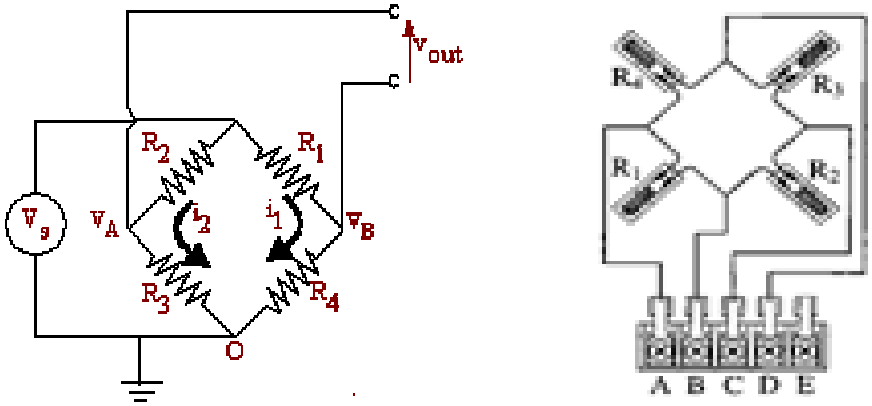

Figure 45. Wheatstone bridge circuit diagram

THIS PAGE INTENTIONALLY LEFT BLANK

APPENDIX D. ACQUISITION PROGRAM MODIFICATION

```
1       !
2       !PROGRAM TO MEASURE THE DRAG AND THRUST OF A
        MINIATURE RAMJET
3       !
4       Xtime=0
6       Lbs_=0
7       For I=1 TO 80
10      Dacu=709
20      Dvm=722
40      ASSIGN @Dacu TO Dacu
50      ASSIGN @Gages TO Dacu
60      ASSIGN @Dvm TO Dvm
80      CLEAR @ Gages
100     CLEAR @ SCREEN
110     CLEAR @ Dacu
320     Id$=VAL$(5)
330     OUTPUT @Dacu;Ac$&Id$
331     Total=0
350     OUTPUT @Dvm;"MEASURE:VOLT:DC? 1V"
360     ENTER @Dvm;Thrust
370     Total=Total+Thrust*(1000)
381     Thrust=Total/5
382     PRIN "THRUST IS ",TAB(27);Thrust;"LBS"
400     CLEAR @ Dacu
420     CLEAR @ Gages
430     ASSIGN @Dacu TO*
450     ASSIGN @Dvm TO*
460     ASSIGN @Gages TO*
461     BEEP
462     PRINT"XTIME =";Xtime,"ITER =";I
464     NEXT I
470     END
```

THIS PAGE INTENTIONALLY LEFT BLANK

APPENDIX E. 2D MODEL FLOW PROBLEM SETUP

Problem Type (PT) : Flow

Under the Model Option (MO) the model is set up as follows:

Global : Asymmetric

Transient : Steady

Flow : Flow Model;

- Gas Model : Ideal Gas

- Viscous Model : Turbulence (Navier-Stokes)

Ideal Gas Properties;

- Molecular Weight : 28.96999931 g/mol

- Gamma (C_p/C_v): 1.399999976

Viscosity : Constant (Dynamic)

- Mu : $1.845999941E^{-05}$ kg/m-s

Conductivity

- Prandtl Number : 0.7

Turbulent Conductivity

- Turb. Prandtl No. : 0.8999999762

Turbulence Model : K Omega

Boundary condition (BC) of the model for the inlet flow flied is defined as follows:

U = 661 ; V = 0 ; W= 0 ; P = 7378 Pa ; T = 68K ; k = 262 ; ω = 65.5

The flow outlet of the model is defined as follows:

Constant Pressure, P= 7378 Pa

The inlet diffuser, the entire casing of the ramjet as well as the top boundary of the model are defined as adiabatic wall and the bottom boundary other than the diffuser are defined as symmetric axis.

Initial Condition (IC) for the entire model is defined as follows:

Fluid :U = 661, V = 0, P = 7378 Pa, T = 68K, k = 262, ω = 65.5

Block :U = 0, V = 0, P = 7378 Pa, T = 68K, k = 262, ω = 65.5

Under the Solver Control (SC) the following parameters were used:

Iteration : 10,000

Spatial : 1st order (Roe's FDS)

- linear wave : 0.2
- non-linear wave : 0.2

Solver :

- Time Iteration : Implicit
- Implicit Scheme : Point Jacobi (Fully Implicit)
- Sub-iteration : 20
- Tolerance : 0.0001

Relaxation :

- Iteration : 1
- Initial CFL : 0.1
- Final CFL : 1
- Ramping Interval : 100

APPENDIX F. 2D MODEL FLOW ANALYSIS RESULTS

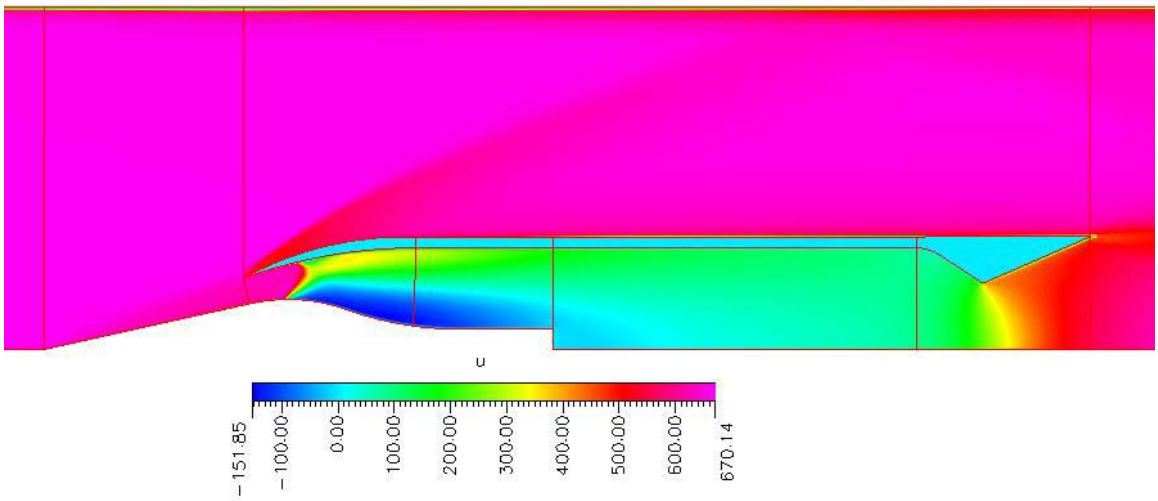

Figure 46. Velocity profile in axial direction at Mach 4.

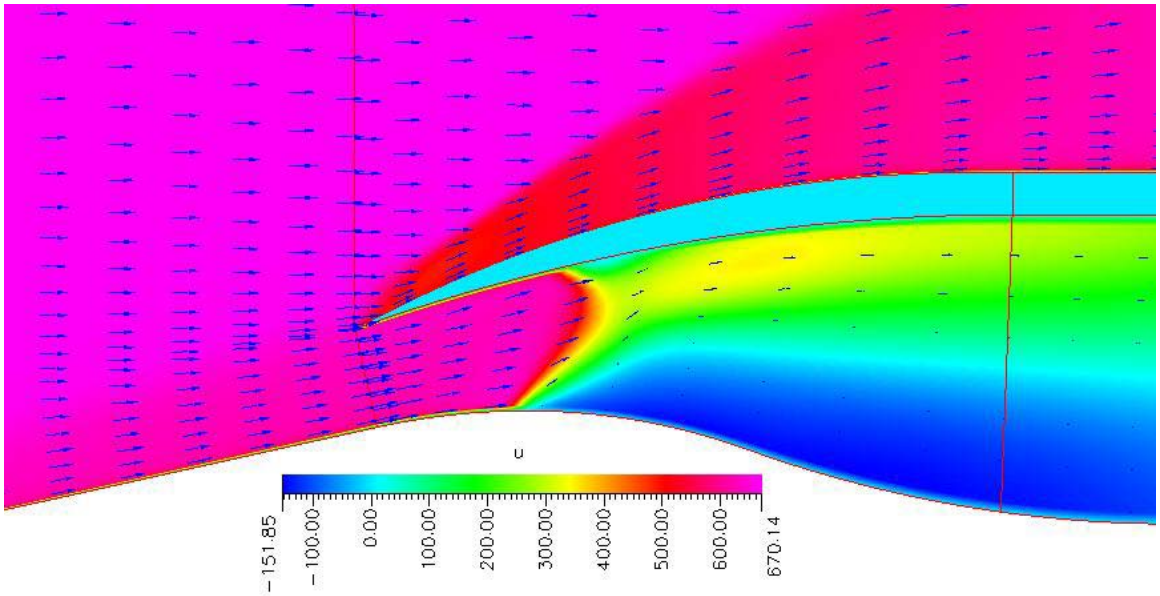

Figure 47. Mach 4 flow field vector at the diffuser inlet.

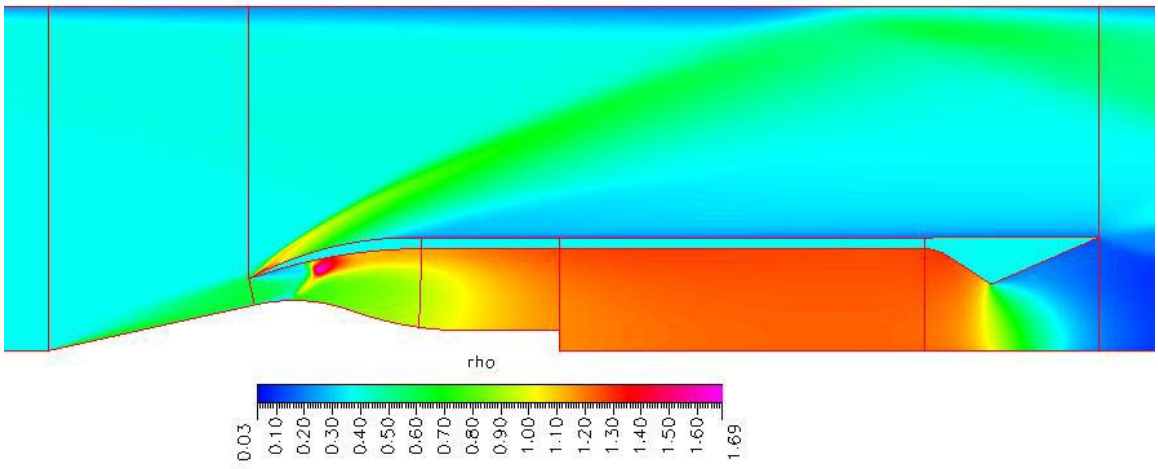

Figure 48. Density distribution profile at Mach 4.

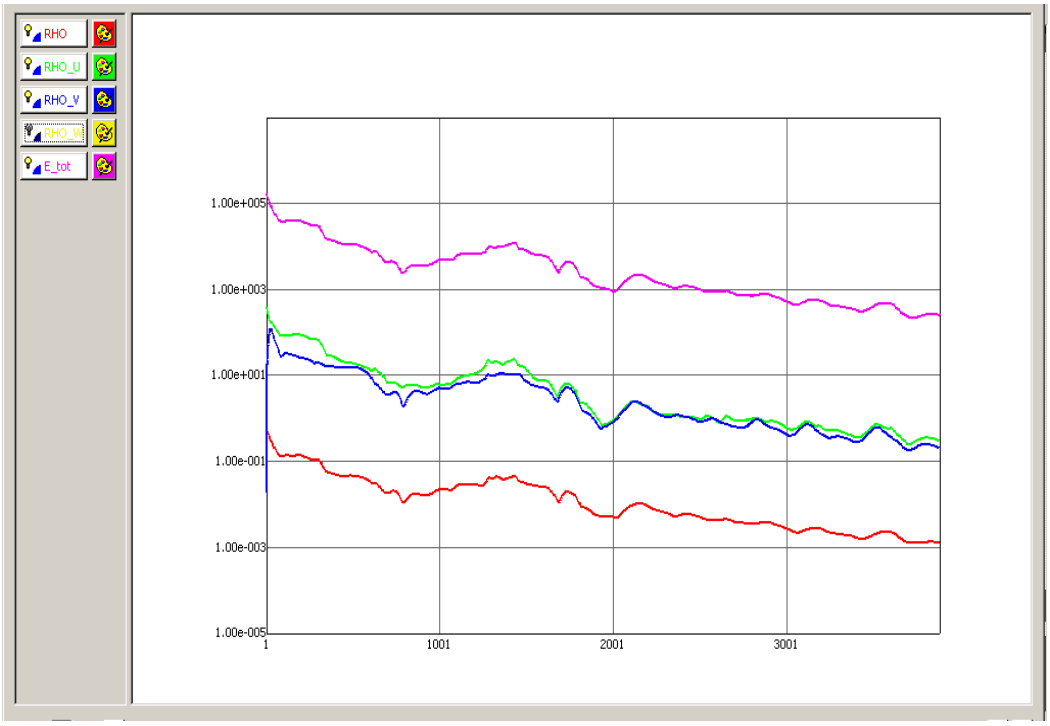

Figure 49. Residual decay as a function of iteration number.

APPENDIX G. FUEL MIXING (164FT/S, 0.02” PORT SIZE)

strut : CFL: 0.05 - 1
U = -7; W = 49
K = 6; Omega = 1980.77
P = 107378; T =300 k
Location: y = 0.0066; z = 0.0065 (Centre of nose injector)

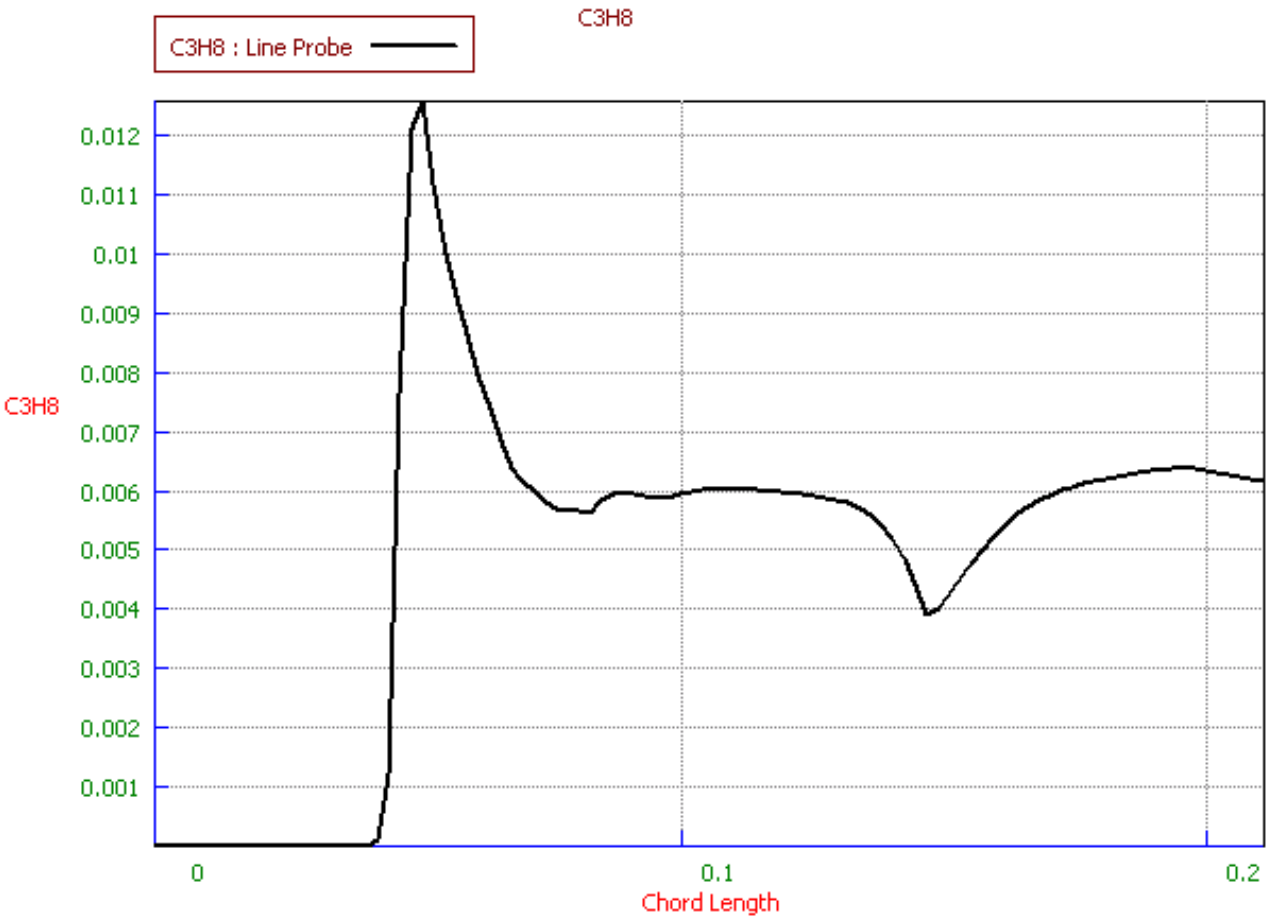

Figure 50. Plot of propane concentration vs axial length for a 0.02” hole with 164ft/s flow rate measured at location 1.

Location: y = 0.0088; z = 0.002 (Centre of strut injector)

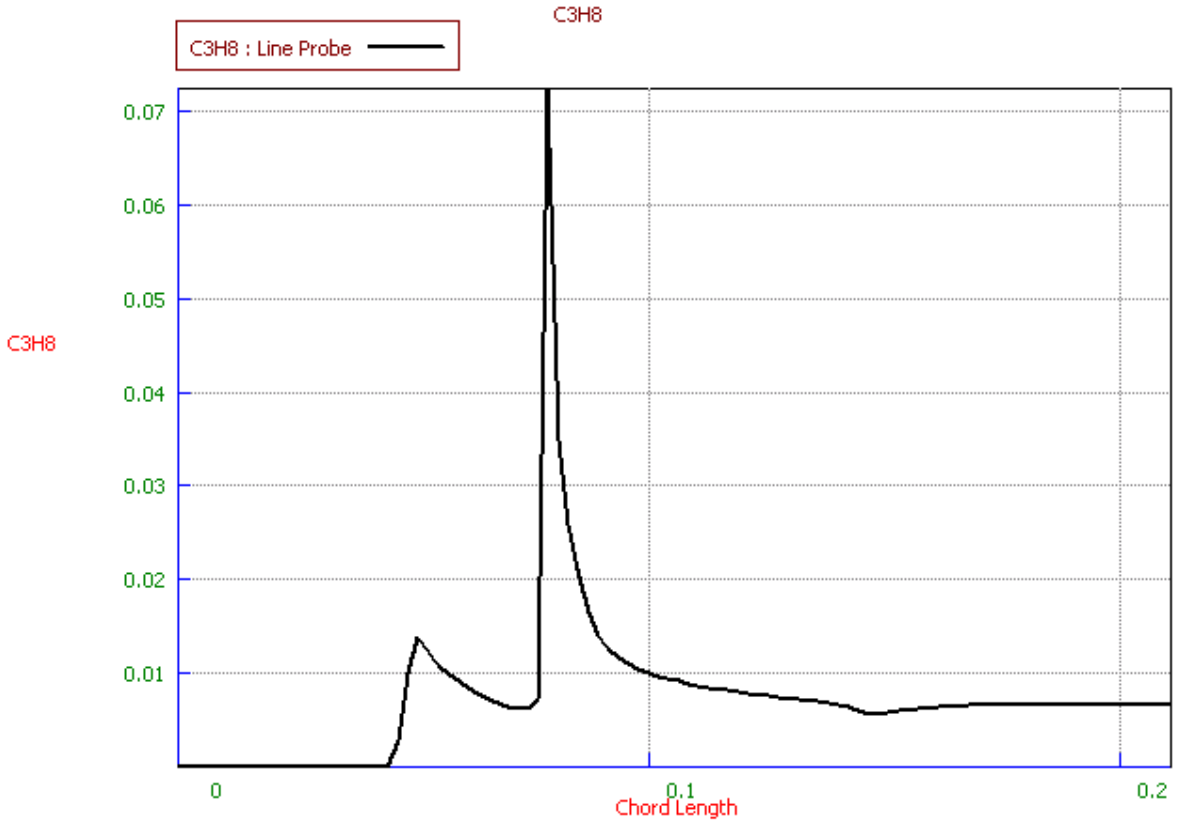

Figure 51. Plot of propane concentration vs axial length for a 0.02” hole with 164ft/s flow rate measured at location 1.

APPENDIX H. FUEL MIXING (164FT/S, 0.05” PORT SIZE)

Strut:
U = -7 CFL : 0.05 - 1
W = 49
P = 107378
T = 300 k
K = 6
Omega = 792

Location: y = 0.0066; z = 0.0065 (near symmetric plan) [164ft/s]

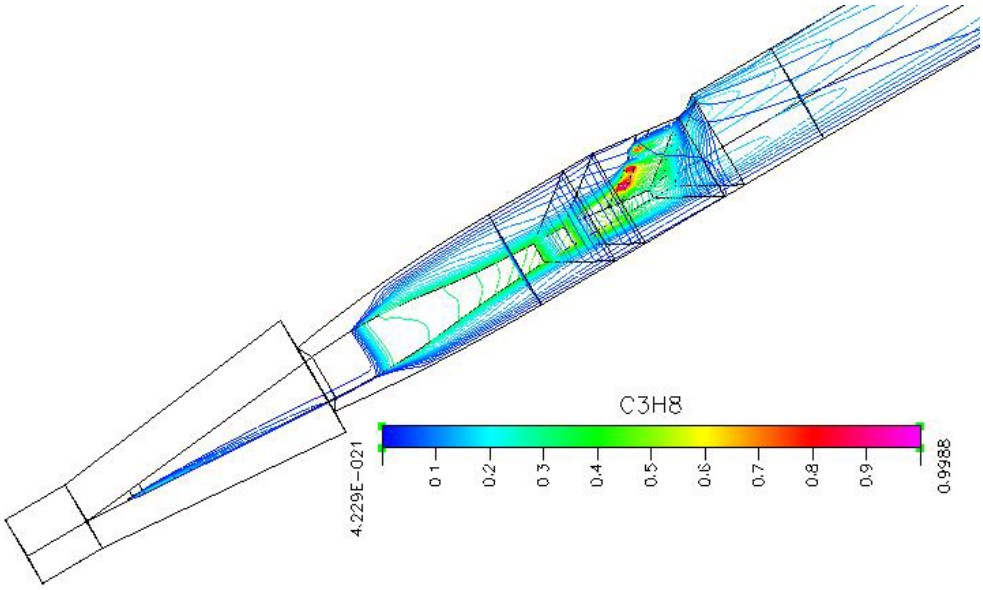

Figure 52. Picture of propane mixing analysis from top view.

Location: y = 0.0088; z = 0.002 (near strut) [164ft/s]]

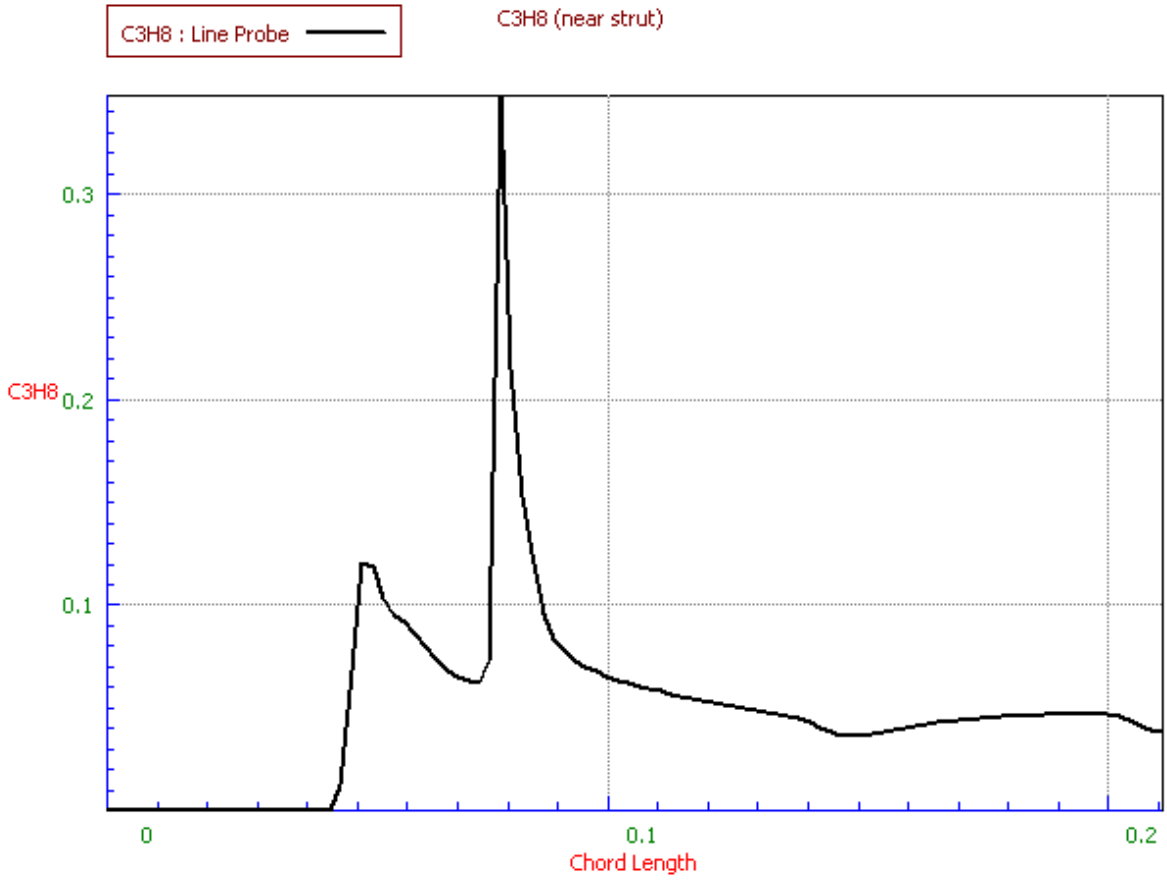

Figure 53. Plot of propane concentration vs axial length for a 0.05” hole with 164ft/s flow rate measured at location 1.

APPENDIX I. FUELMIXING (246FT/S, 0.05” PORT SIZE)

Strut :
U = -10.85 mps
W = 74.2 mps
P = 107378
T = 300 k
K = 3.375
Omega = 594.23

CFL : 0.05 – 2 (iteration 1- 2781)
CFL : 0.05 – 1 (iteration 2782 - 3754)
Residuals: 4 order drops

Location: y = 0.0066; z = 0.0065 (near symmetric plan) [246ft/s]

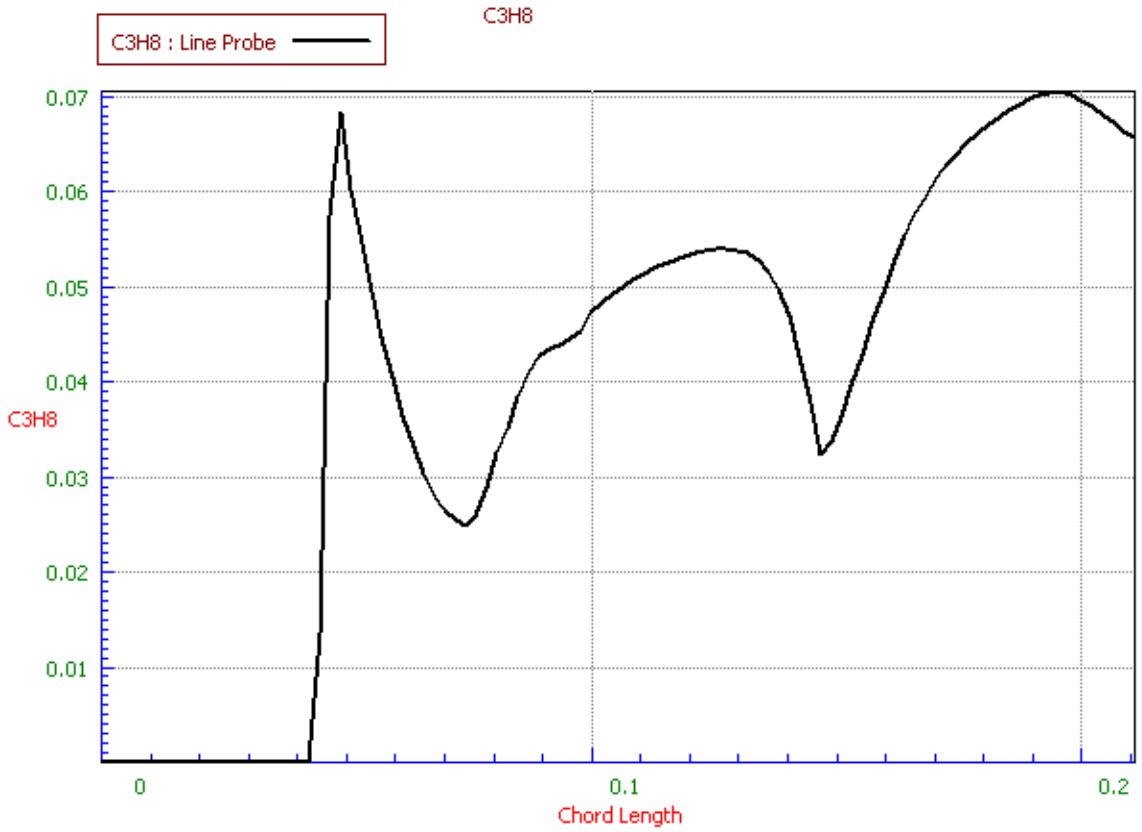

Figure 54. Plot of propane concentration vs axial length for a 0.05” hole with 246ft/s flow rate measured at location 1.

Location: y = 0.0088; z = 0.002 (near strut) [246ft/s]

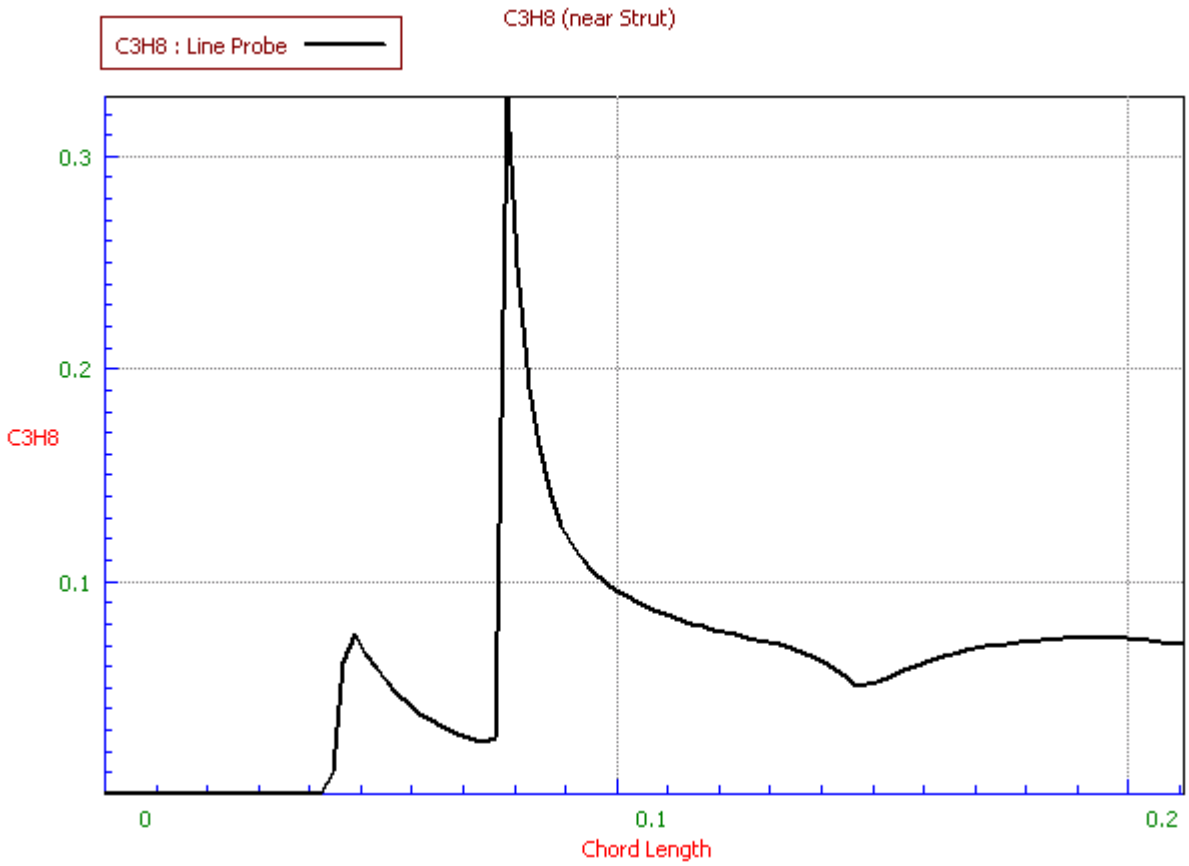

Figure 55. Plot of propane concentration vs axial length for a 0.05” hole with 246ft/s flow rate measured at location 1.

APPENDIX J. FUEL MIXING (328FT/S, 0.05” PORT SIZE)

Strut :
U = -14.5 mps
W = 99 mps
P = 107378
T = 300 k
K = 6
Omega = 792.3

CFL : 0.05 – 2

Residuals: 4 order drops

Location: y = 0.0066; z = 0.0065 (near symmetric plan) [328ft/s]

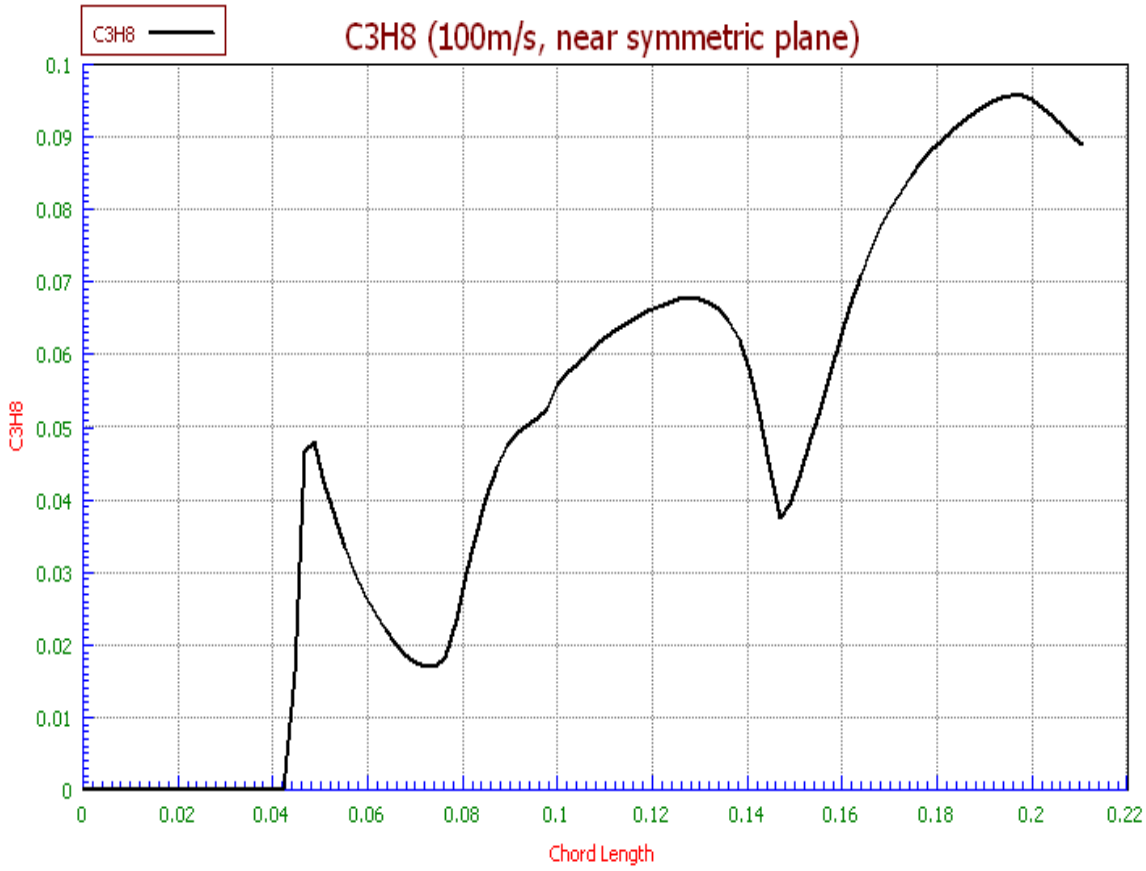

Figure 56. Plot of propane concentration vs axial length for a 0.05” hole with 328ft/s flow rate measured at location 1.

Location: y = 0.0088; z = 0.002 (near strut) [328ft/s]

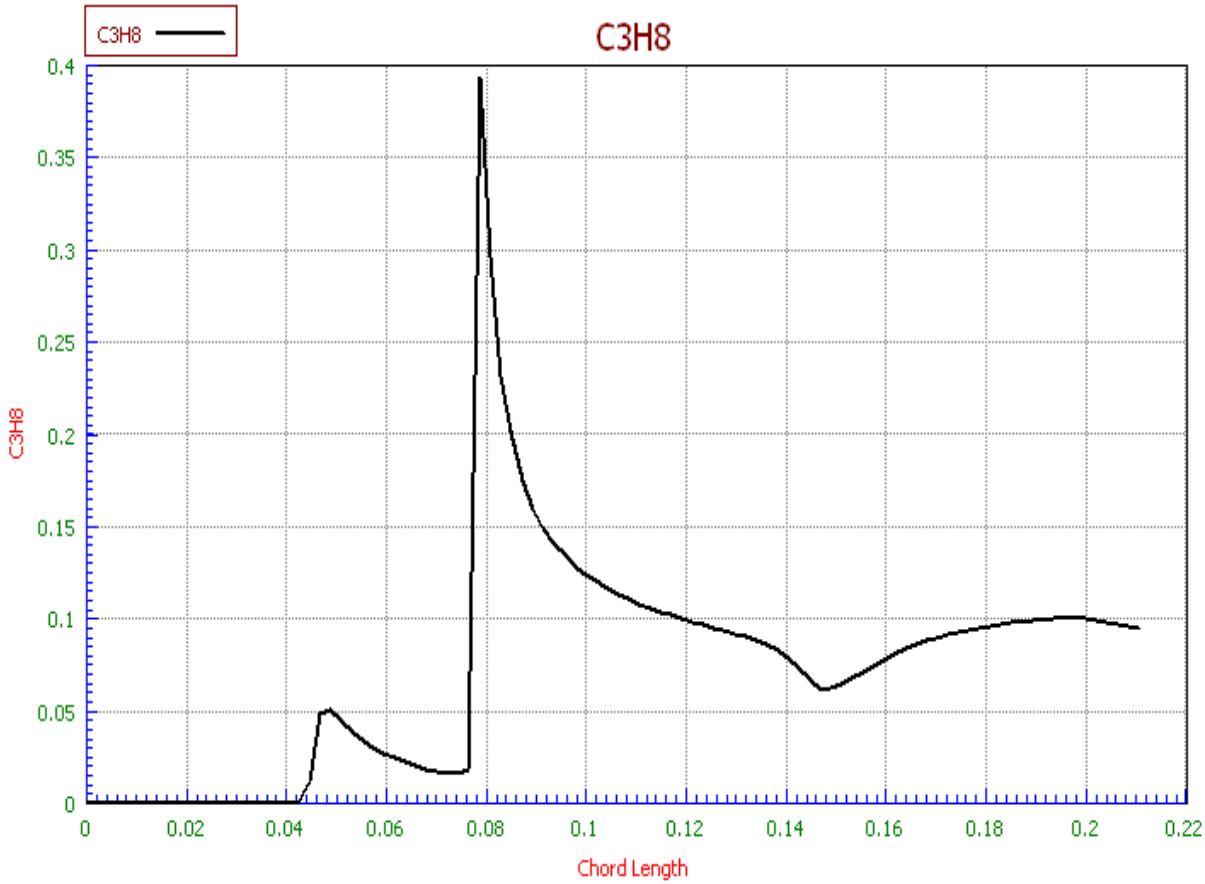

Figure 57. Plot of propane concentration vs axial length for a 0.05” hole with 328ft/s flow rate measured at location 1.

APPENDIX K. FUEL MIXING (410FT/S, 0.05” PORT SIZE)

Strut :
U = -18.06 mps
W = 123.68 mps
P = 107378
T = 300 k
K = 9.375
Omega = 990.38

CFL : 0.05 – 21

Residuals: 4 order drops

Location: y = 0.0066; z = 0.0065 (near symmetric plan) [410ft/s]

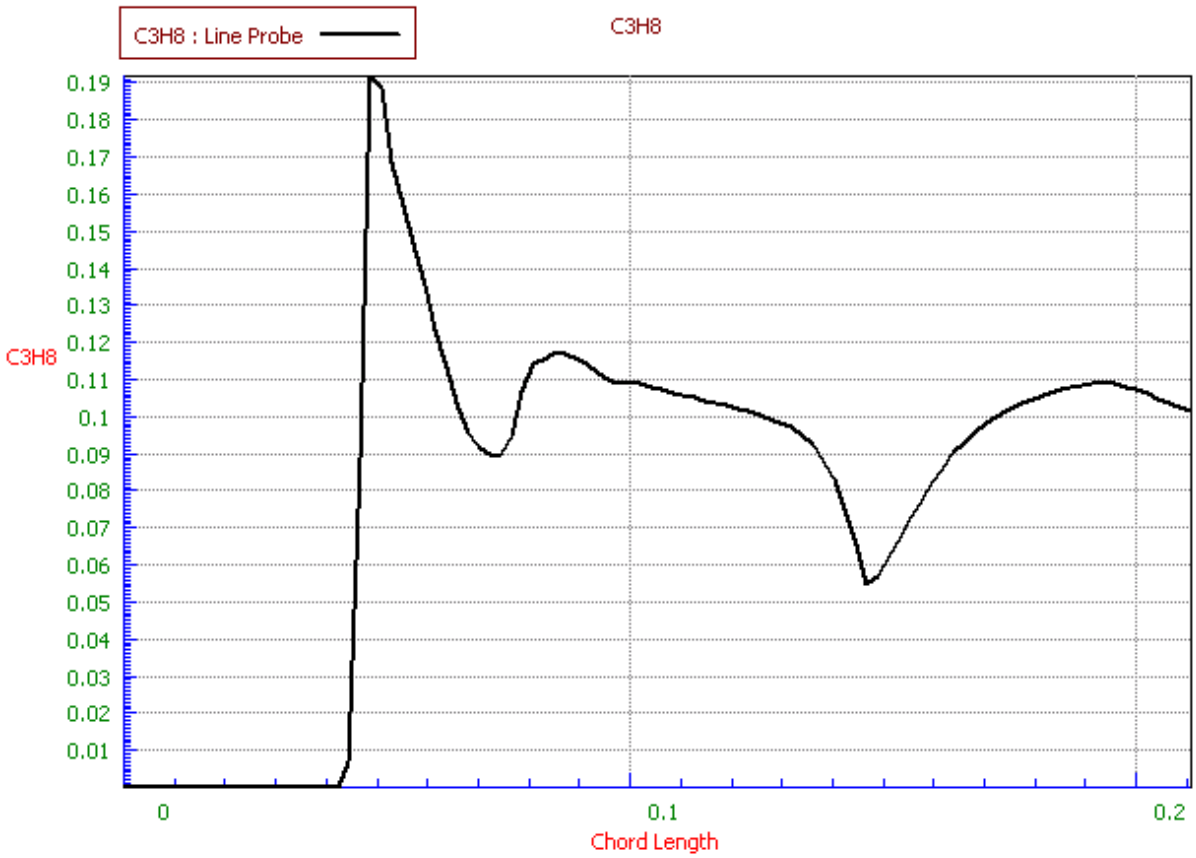

Figure 58. Plot of propane concentration vs axial length for a 0.05” hole with 410ft/s flow rate measured at location 1.

Location: y = 0.0088; z = 0.002 (near strut) [410ft/s]

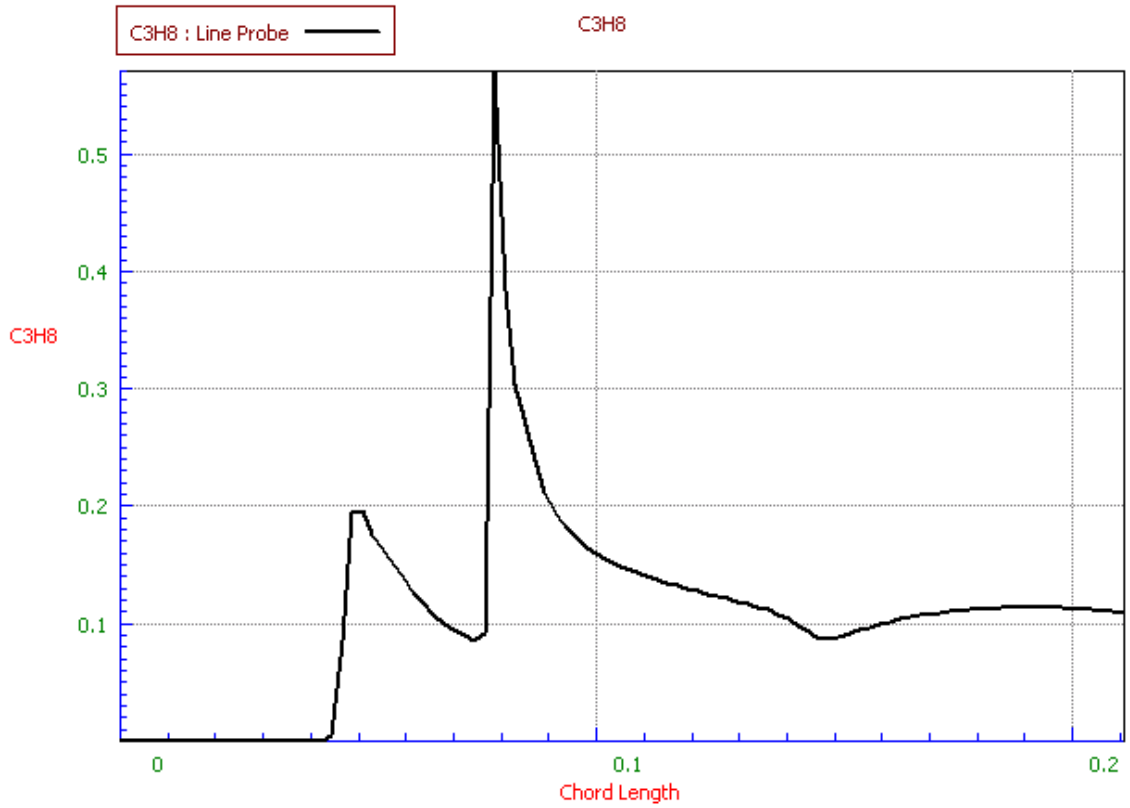

Figure 59. Plot of propane concentration vs axial length for a 0.05” hole with 410ft/s flow rate measured at location 1.

APPENDIX L. 2D COMBUSTION MODEL SETUP

Problem Type (PT) : Flow, Heat Transfer, Turbulence, Chemistry

Under the Model Option (MO) the model is set up as follows:

Shared : Asymmetric

Flow : Ref. Pressure = 0

Heat : Do not tick

Turb : K-omega, 0.9, 0.9

Chem :

- Chemistry Media : Gas Phase
- Gas Phase : Species mass fraction

Under the Volume Conditions (VC) the model is set up as follows:

Shared :

- Density : Ideal Gas Properties;
- Viscosity : Mix Sutherland's law

Heat :

- Mix JANNAF Method
- Prandtl Number

Chem :

- Schmidt Number : 0.7

Under the Boundary Conditions (BC) the model is set up as follows:

BC of the model for the inlet flow flied is defined as follows:

Air; U = 15 ; V = 0 ; P = 7378 Pa ; T = 300K ; k = 0.135 ; ω = 1.5

Propane; U = 1, V = 0; P = 7378 Pa; T = 1200K; k = 6E-4; ω = 8

The flow outlet of the model is defined as follows:

Constant Pressure, P= 7378 Pa

The inlet diffuser, the entire casing of the ramjet as well as the top boundary of the model are defined as adiabatic wall and the bottom boundary other than the diffuser are defined as symmetric axis.

Initial Condition (IC) for the entire model is defined as follows:

Fluid :U = 2, V = 0, P = 7378 Pa, T = 300K, k = 0.135, ω = 1.5, Air

Under the Solver Control (SC) the following parameters were used:

Iteration : 4,000

Convergence Crit. : 0.000001

Min Residual : 1E-018

Spatial : Upwind

Relax :

- Velocities : 0.2
- P correction : 5

- Enthalpy : 0.2

- Turbulence : 0.2

- Species : 0.05

Once the converge solution was attained, activate the combustion model by :

Under the Model Option (MO) the model is set up as follows:

Chem :

- Chemistry Media : Gas Phase

- Gas Phase : Species mass fraction

tick the gas phase reaction

under Define;

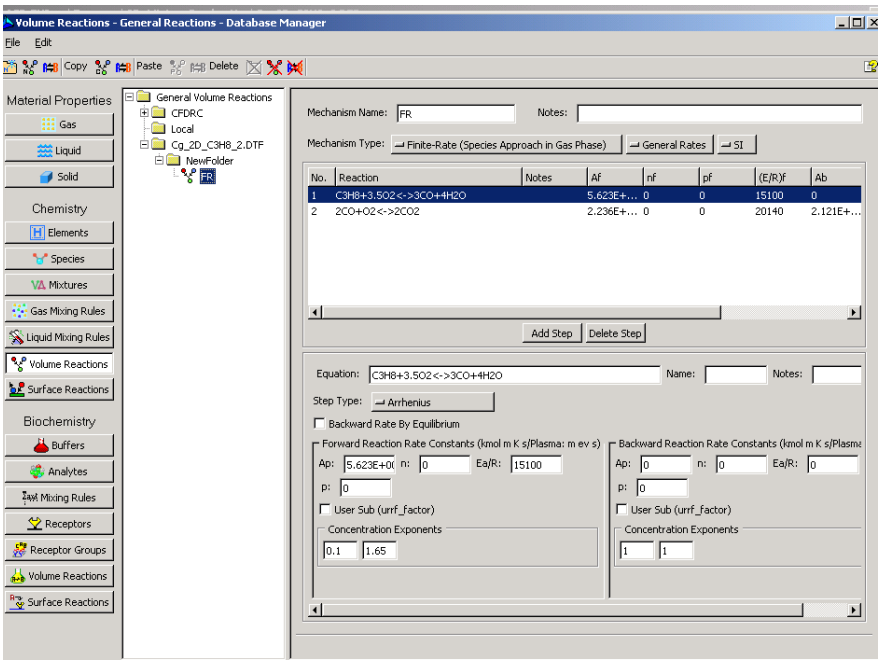

THIS PAGE INTENTIONALLY LEFT BLANK

LIST OF REFERENCES

1. W.H. Heiser, United States Air Force Academy, D. T. Pratt, University of Washington, *Hypersonic airbreathing propulsion*, AIAA education series, 1994.

2. J. W. Snyder, Aerospace Engineer, U.S. Army TACOM-ARDEC, MAJ K. M. Nash, Armor systems officer, U.S. Army TACOM-ARDEC, *A scramjet propulsion system for gun-launched kinetic energy penetrators,* Jan 2002.

3. K. M. Ferguson, *Design and clod flow evaluation of a miniature Mach 4 ramjet*, Master's Thesis, Department of Aeronautics and Astronautics, U.S. Naval Postgraduate School, Monterey, CA, June 2003.

4. *CFDRC FASTRAN User and Theory manual,* 2003.

5 Wilcox D.C., *Turbulence Modeling for CFD, D.C.W*. Industries Inc, 1993

6. D. A. Perretta, *Laser doppler velocimetry measurements across a normal shock in transonic flow*, Master's Thesis, Department of Aeronautics and Astronautics, U.S. Naval Postgraduate School, Monterey, CA, March 1993

7. *CFDRC ACE User manual,* 2003.

THIS PAGE INTENTIONALLY LEFT BLANK

INITIAL DISTRIBUTION LIST

1. Defense Technical Information Center
   Ft. Belvoir, Virginia

2. Dudley Knox Library
   Naval Postgraduate School
   Monterey, California

3. Professor Anthony J. Healey
   Chairman, Department of Mechanical and Astronautical Engineering
   Naval Postgraduate School
   Monterey, California

4. Professor Garth V. Hobson
   Naval Postgraduate School
   Monterey, California

5. Professor Raymond P. Shreeve
   Naval Postgraduate School
   Monterey, California

6. Naval Air Warfare Centre Aircraft Division
   Propulsion and Power Engineering
   Patuxent River, MD
   ATTN: C. Georgia, Code 4.4

7. Naval Air Warfare Centre Weapons Division
   China Lake, CA
   ATTN: J. Moore, Code 477400D

8. Professor Yeo Tat Soon
   Director, Temasek Defence System Institute
   National University of Singapore
   Singapore